Article:
Kempf, Michael, Luterbacher, Jürg, Petrik, Jan et al. (2026) Adaptive connectivity networks across climatic and ecological regimes from the Neolithic to the Middle Ages in the Carpathian Basin. Quaternary Science Reviews. 110152. ISSN: 0277-3791

https://doi.org/10.1016/j.quascirev.2026.110152

Quaternary Science Reviews 389 (2026) 110152

Contents lists available at ScienceDirect

Quaternary Science Reviews

journal homepage: www.elsevier.com/locate/quascirev

Adaptive connectivity networks across climatic and ecological regimes from the Neolithic to the Middle Ages in the Carpathian Basin

Michael Kempf[a,*], Jürg Luterbacher[b], Jan Petrik[c], Ulf Büntgen[a,d,e], Penny Bickle[f], Attila Kreiter[g], Elena Xoplaki[h], Margaux L.C. Depaermentier[i]

[a] Department of Geography, University of Cambridge, Cambridge, UK
[b] Department of Geography and Liebig Centre for Agroecology and Climate Impact Research, Justus Liebig University of Giessen, Justus Liebig University Giessen, Giessen, Germany
[c] Department of Geological Sciences, Faculty of Science, Masaryk University, Brno, Czech Republic
[d] Global Change Research Institute (CzechGlobe), Czech Academy of Sciences, Brno, Czech Republic
[e] Department of Geography, Faculty of Science, Masaryk University, Brno, Czech Republic
[f] Department of Archaeology, University of York, The King's Manor, York, UK
[g] Archaeometry Laboratory, Hungarian National Museum, Budapest, Hungary
[h] CMCC Foundation – Euro-Mediterranean Centre on Climate Change, Bologna, Italy
[i] Faculty of History, Vilnius University, Vilnius, Lithuania

A R T I C L E I N F O

Handling Editor: Donatella Magri

A B S T R A C T

Investigating long-term archaeological land-use patterns is crucial for understanding how past populations adjusted settlement strategies, resource exploitation, and communication networks in response to environmental and climatic variability. Recent quantitative archaeological research has provided important insights into long-term spatio-temporal social transformations in the Carpathian Basin. Yet the diachronic relationships between communication networks and environmental and climatic changes remain poorly understood. To fill this gap, we present a standardized, transparent, and replicable framework to compare relative connectivity across distinct site-distribution patterns, using a center–periphery model derived from custom network analyses spanning the Neolithic to the Hungarian Conquest period (~8000–1000 BP). We develop and present climatically adjusted and simulated movement networks based on spatially clustered centers, emphasising high site intensities and travel cost efficiency derived from a weighted walking friction model incorporating topography and hydrology. We further compare land-use patterns and socio-ecological persistence with crop cultivation strategies based on carbon and nitrogen stable isotope data from human and animal remains. Our results show period-specific differences in centre–periphery structures and accessibility inequalities, alongside changing associations between archaeological footprints and descriptive environmental classes. These patterns are consistent with repeated reorganisation under changing environmental conditions, rather than with a uniform response to environmental change.

1. Introduction

The Carpathian Basin serves as a communication corridor throughout prehistory, governed by its distinctive geography and major hydrological systems (Bánffy, 2019; Gaudenyi and Mihajlović, 2022; Kempf, 2021; Magyari et al., 2024). Over time, culturally diverse human groups and societies created a wide range of settlement patterns and interaction landscapes, producing a complex palimpsest of communication networks and exchange routes (Kempf, 2020, 2021). Understanding the factors that shaped these connectivity systems and how they evolved over time is crucial for interpreting long-term socio-cultural transformations, including shifts in individual mobility, subsistence strategies, larger trade routes, and the location of central hubs. Although the Holocene is often considered as climatically more stable

* Corresponding author.
E-mail addresses: mk2145@cam.ac.uk (M. Kempf), juerg.luterbacher@geogr.uni-giessen.de (J. Luterbacher), petrik.j@sci.muni.cz (J. Petrik), ulf.buentgen@geog.cam.ac.uk (U. Büntgen), penny.bickle@york.ac.uk (P. Bickle), kreiter.attila@hnm.hu (A. Kreiter), elena.xoplaki@cmcc.it (E. Xoplaki), margaux.depaermentier@if.vu.lt (M.L.C. Depaermentier).

https://doi.org/10.1016/j.quascirev.2026.110152
Received 17 March 2026; Received in revised form 24 June 2026; Accepted 25 June 2026
Available online 27 June 2026

than earlier periods (Brown et al., 2013), it was nevertheless characterized by pronounced climatic regime shifts and periods of increased hydroclimatic extremes. Despite major advances in environmental and quantitative archaeology in the study area particularly in research on population dynamics, land-use, and site-distribution patterns (Depaermentier et al., 2020a,b; Depaermentier et al., 2020a,b2021, 2025a; Fort, 2022; Kempf, 2020, 2021; Kempf and Günther, 2023; Magyari et al., 2024), most studies of spatial-diffusion and connectivity have focused on individual periods within the Holocene, making it difficult to determine whether the observed structures are period-specific or reflect long-term spatial persistence.

We present a custom developed modelling approach for diachronic comparison of archaeological site distribution, network connectivities, movement corridors (e.g. Verhagen et al., 2019; Collar et al., 2015; Brughmans, 2013; Petrie et al., 2026) and environmental conditions from the Neolithic period to the Middle Ages (~8000–1000 BP). Using this approach, we aim to capture both the centrality structure and the hinterland integration of the Carpathian Basin (Fig. 1). By integrating the custom-derived ecological zonation model developed by Kempf (2026), we further evaluate the relationship between archaeological core area distributions and ecological conditions across the Carpathian Basin (Kempf, 2026a, 2021). A comparison with published stable carbon and nitrogen isotope data derived from human and animal remains further offers the possibility to explore the link with shifts in subsistence practices (Lee-Thorp, 2008). This paper thus provides a workflow for environmentally and climatologically weighted network simulations and comparative spatial analysis that can also be applied to other regions with dense archaeological records beyond the study area. The framework complements recent work that has examined climatic constraints on Neolithic expansion (Betti et al., 2020) and environmentally differentiated mobility corridors (Petrie et al., 2026). Rather than modelling agricultural suitability or spatially explicit paleoclimatic gradients, this study compares centre–periphery configurations under a terrain–hydrology friction surface modified by a period-specific hydroclimatic index.

2. Modern environmental and climate settings

The Carpathian Basin is situated in East-Central Europe and forms a topographically enclosed lowland surrounded mostly by the Carpathians Mountains and dominated by the two major river systems of the Danube and the Tisza (Fig. 1). Present-day seasonal temperatures are highest in summer (June-August), which coincide with the season with most rainfall (mostly convective). During the winter months (December-February), the strongly continental climate brings cold and dry conditions to most parts of the Carpathian Basin. The region is primarily governed by large-scale atmospheric circulation reflecting the interaction between Atlantic, Mediterranean, and continental influences. Enhanced Atlantic westerly flow is generally associated with milder conditions and increased precipitation, particularly on the western and northern flanks of the Carpathians, while Mediterranean cyclones provide episodic but often dominant contributions to heavy precipitation and flood events, especially during spring and autumn. In contrast, circulation regimes characterised by blocking over eastern Europe and western Russia favour the advection of dry continental air masses, leading to persistent cold spells in winter as well as heatwaves and drought in summer. During the cold season, precipitation variability is strongly modulated by the phase of the North Atlantic Oscillation, with negative phases favouring enhanced moisture transport towards southern and south-eastern Europe and increased precipitation in the Carpathian region (Ionita, 2014; Perşoiu et al., 2017). Winter precipitation regimes are further shaped by the interaction between Atlantic and Mediterranean moisture pathways and persistent continental anticyclones over western Russia, which can suppress precipitation and prolong anomalous conditions (Perşoiu et al., 2019).

3. Paleoclimatic evidence

The Holocene experienced several pronounced climatic excursions across the Northern Hemisphere (McKay et al., 2024 and references therein) with the 8.2 ka cal BP event being the most prominent rapid cooling episode associated with changes in precipitation regimes (Alley and Agustsdottir, 2005; McKay et al., 2024; Morrill et al., 2013; Parker and Harrison, 2022). High resolution speleothem records from Cloşani Cave in southwestern Romania demonstrated that autumn and winter precipitation during the early to mid-Holocene was substantially higher than present, with anomalies of up to 80% during the 8.2 ka event (Warken et al., 2024) (Fig. 2). In addition, Feurdean et al. (2008) reported the 8.2 ka cal BP event as one of the most prominent Holocene excursions in the Carpathian Basin, associated with reduced winter and spring temperatures and increased summer temperatures, potentially enhancing continentality (Feurdean et al., 2008; Seppä et al., 2007). Contrasting summer cooling signals from the eastern Carpathians (Perşoiu et al., 2017) and the strong precipitation increase documented

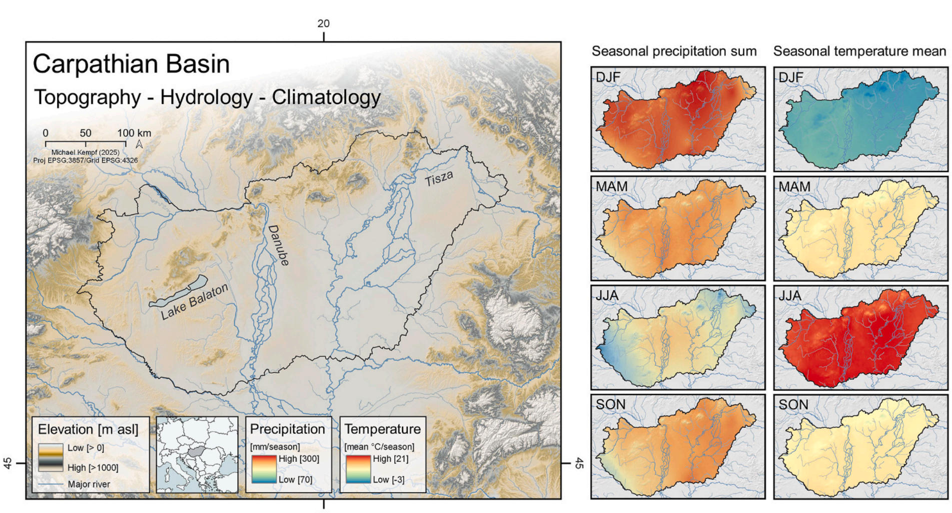

Fig. 1. Present-day environmental and climatological settings of the study area. Topography (m asl) (OpenTopography, 2013), hydrology (major river systems (European Environment Agency, 2019)), and climatology (precipitation (mm/season); temperature (mean/season), reference period 1970-2000 (Fick and Hijmans, 2017)); DJF = December-February; MAM = March-May; JJA = June-August; SON=September-November) in the Carpathian Basin and modern day Hungary (black polygon).

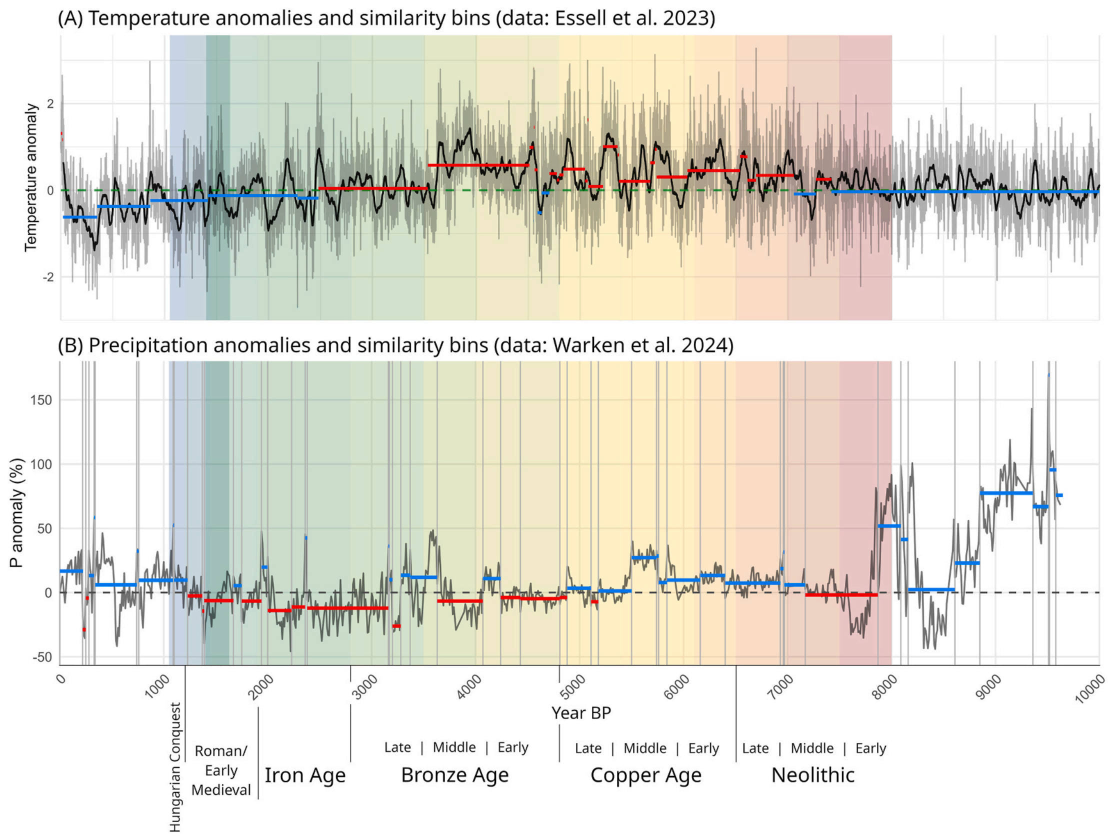

Fig. 2. Holocene temperature anomalies (A) and precipitation (B) anomalies and climatic similarity phase bins during the Holocene. (A) Dynamic temperature similarity bins with a threshold of *mean*(*ts*)+4**SD*(*ts*) across the annually resolved timeseries (*ts*): cold (blue) and warm (phases); green dashed line marks the mean (0) and the black line is the rolling window mean (n = 50 years); data from Essell et al. (2023). (B) Precipitation anomalies of Closani (Romania) composite speleothem records based on Warken et al. (2024); similarity bins with a local threshold of *mean*(*ts*)+2**SD*(*ts*) across the discontinuous time series. (For interpretation of the references to colour in this figure legend, the reader is referred to the Web version of this article.)

by speleothems highlight the spatial heterogeneity of the 8.2 ka event outside the North Atlantic core region, consistent with findings by McKay et al. (2024). This event potentially contributed to the onset of the Neolithic transition into Thrace, Macedonia, Thessaly, Bulgaria (Weninger et al., 2006). While in the Lower Danube the 8.2 ka climatic event likely brought cooler and wetter conditions, increasing river discharge and flooding, Mesolithic hunter-gatherer communities were forced to adjust their settlement patterns and mobility strategies (Bonsall et al., 2015).

Beyond the 8.2 ka event, Holocene hydroclimatic variability in Eastern Central Europe appears to have been largely governed by dynamic atmospheric processes rather than thermodynamic forcing alone (Warken et al., 2024). This includes mid Holocene anomalies such as the 7.2 ka event identified by Hou et al. (2023), whose regional expression remains heterogeneous (Hou et al., 2023). Despite the supposed relative stability during the middle Holocene, multiple proxy records from Romania document repeated short-term hydroclimatic oscillations and changes in precipitation variability (Bodnariuc et al., 2002; Feurdean et al., 2008; Perşoiu et al., 2017; Warken et al., 2024). The Cloşani Cave record indicates that autumn and winter precipitation between approximately 9.5 and 4 ka BP was on average 20 to 30% higher than present day levels, with episodic extremes exceeding this range (Warken et al., 2024). After approximately 4.7 ka cal BP, hydroclimatic conditions in the Carpathian region became increasingly variable, with the late Holocene marking a period of more frequent extremes (Warken et al., 2024). This variability is interpreted as a consequence of changes in North Atlantic sea level pressure patterns, increased atmospheric blocking, and shifts in jet stream dynamics rather than gradual temperature forcing alone.

The 4.2 ka event, approximately 4300 to 3900 yr BP marks the boundary between the middle and late Holocene and has traditionally been associated with widespread drought and societal transformations (Nan et al., 2025 and references therein). However, recent global and regional analyses demonstrate that the 4.2 ka event lacks the spatial coherence observed for the 8.2 ka event, and is instead characterized by pronounced hydroclimatic heterogeneity (McKay et al., 2024; Nan et al., 2025, 2026). For the Carpathian region, this heterogeneity is particularly evident. While winter megadroughts have been documented in parts of the Mediterranean Basin, speleothem and lake records from Romania indicate generally wetter conditions, increased runoff, and low wildfire activity between approximately 4.7 and 3.3 ka BP, with especially wet phases after 4.3 ka BP (Feurdean et al., 2013; Panait et al., 2017; Perşoiu et al., 2017). Warken et al. (2024) showed that this period coincides with higher precipitation variability and a growing influence of dynamic circulation processes, including atmospheric blocking and jet stream reorganisation, rather than with a uniform drying signal. Although uncertainties regarding the synchronicity of hydroclimatic changes across Europe were already raised by Wanner et al. (2008), glacier advances indicate phases of Northern Hemisphere cooling between 3.8 and 3.1 ka BP and between 3.0 and 2.3 ka BP (Seppä et al., 2009; Wanner et al., 2008). These cooler intervals were followed by a long-lasting warming trend peaking around 2.0 ka BP, commonly referred to as the Roman Warm Period in Central Europe (Seppä et al., 2009).

The subsequent Medieval period was characterized by pronounced climatic variability across Europe, with alternating phases of cooling, warming, and changes in hydroclimatic conditions. One of the most prominent intervals was the Late Antique Little Ice Age (LALIA), a cooling period that started following the 536/537 and 540 CE volcanic events (Büntgen et al., 2016; Helama et al., 2017; Van Dijk et al., 2022). This period is reflected in widespread temperature reduction and changes in the hydrological cycle in many parts of Europe and the Mediterranean (Xoplaki et al., 2021). During the Early Medieval period, relatively warmer conditions have been reported in Northern Europe, in contrast to colder conditions in Central and Southwestern Europe (Luterbacher et al., 2016). The Medieval Climate Anomaly (MCA) represents another major interval of Medieval climate variability, although its expression is spatially and seasonally heterogeneous. In Europe, the MCA is most clearly expressed in summer temperature reconstructions, particularly in western and northern regions (Bradley et al., 2003; Goosse et al., 2006; Graham et al., 2011; Luterbacher et al., 2016). In Central, Southern and Eastern Europe, including the Carpathian Basin, the signal appears more complex, with weaker or less consistent temperature anomalies (Luterbacher et al., 2016) and a stronger role of hydroclimatic variability and atmospheric circulation changes (Xoplaki et al., 2016, 2018, 2021). Tree-ring evidence from the Eastern Carpathians is consistent with this interpretation: a summer mean temperature reconstruction from the Călimani Mountains spanning 1163–2005 CE does not show a clearly sustained Medieval warm phase, but instead indicates relatively modest Medieval summer-temperature anomalies compared with western and northern Europe (Popa and Kern, 2009). For the subsequent centuries, regional tree-ring records provide clearer evidence of climatic variability. The same reconstruction identifies a pronounced Little Ice Age summer-cooling signal between 1370 and 1630 CE, followed by lagged cold decades around 1820 and 1840 CE (Popa and Kern, 2009). A tree-ring cellulose δ^{18}O-based August SPEI3 reconstruction from the Eastern Carpathians for 1331–2012 CE likewise indicates a higher frequency of wet years during 1500–1850 CE and a shift toward drier conditions after about 1850 CE, linked to higher summer geopotential heights over central and eastern Europe (Nagavciuc et al., 2022). Additional tree-ring hydroclimate reconstructions from Romania further underline the importance of moisture variability and circulation forcing in the wider Carpathian region, including an April–June hydroclimate reconstruction from a regional beech network extending back to 1768 CE and a summer drought reconstruction from southwestern Romania extending back to 1688 CE (Levanič et al., 2013; Roibu et al., 2022). These records indicate that medieval and post-medieval climate variability in the Carpathian region is expressed through coupled summer-temperature and hydroclimatic signals, with moisture conditions strongly modulated by large-scale atmospheric circulation.

4. Material and methods

4.1. Archaeological datasets

The metadata and location of the sites used in this paper were provided by the administrators of the Archaeology Database (https://archeodatabase.hnm.hu/en) of the Hungarian National Museum and are available upon request from the administrators. The Archaeology Database is an online catalogue of Hungarian archaeological sites that includes both metadata, excavation documentations and scientific reports (Kreiter, 2021). For these reasons, only the major, well-defined phases (Neolithic to Hungarian Conquest period) were included into the analysis and merged to broader chronological periods: Neolithic period (c. 8000–6900 BP, n = 5177), Copper Age (c. 6900–4600 BP, n = 4406), Bronze Age (c. 4800/4600–2800 BP, n = 10047), Iron Age (2800–1900 BP, n = 4075), Roman/Early Medieval period (2100/1900 – 1100 BP, n = 11602), Hungarian Conquest period (~/1200/1150 – 1050 BP, n = 1154) (Supplementary Fig. S1). A fully reproducible and synthetic model to replicate similar results can be accessed from Kempf (2026b). Experimental code and data is available from Kempf (2026c).

4.2. Environmental datasets

A Digital Elevation Model (DEM) derived from SRTM 90 v.4.1 tiles (NASA Shuttle Radar Topography Mission (SRTM) (2013), distributed by OpenTopography; https://doi.org/10.5069/G9445JDF, accessed 2025-07-05). Available for download in tiles measuring 5 by 5° in longitude and latitude, this dataset comes with a resolution of 3 arc seconds, equivalent to a nominal resolution of 90 m at the equator. The DEM was resampled to a 250 m resolution in a meter-based coordinate system (EPSG:3857) to preserve large and moderate terrain properties and to reduce computational expenses.

4.3. Palaeoclimate data

Annually resolved temperature anomalies derived from the composite presented in Essell et al. (2023) (Fig. 2, upper panel), which covers the past ten thousand years (Essell et al., 2023). To reduce high-frequency noise while retaining centennial-scale variability, the time-series (ts) was aggregated into consecutive 10-year bins using mean values. Climatic phases were identified using a similarity-based dynamic binning approach (Kempf et al., 2025), whereby new phase boundaries were defined when absolute annual temperature changes exceeded a threshold calculated as the $mean(ts) + 4*SD(ts)$ across ts. Mean temperature values were calculated for each resulting segment. The temperature reconstruction is used to characterise the broader Holocene climatic context and to support the phase presentation in Fig. 2. The climate weighting applied in the network model is based on the precipitation-derived hydroclimatic index described below.

Precipitation anomalies were reconstructed from two stalagmites (C09-1 and C09-2) from Cloşani Cave following the trace-element–based methodology of Warken et al. (2024) and the methods described in the supplementary information (Fig. 2, lower panel). The Mg/Ca time-series were smoothed using a 5-year linearly weighted running mean as implemented by Warken et al. (2024). Absolute differences in Mg/Ca between the two stalagmites were corrected using a standardized overlap approach, in which C09-1 was normalized and rescaled to the mean and variance of C09-2 over their common interval. A composite Mg/Ca record was then constructed by preferentially using C09-2 where available and scaled C09-1 elsewhere. Composite Mg/Ca values were converted to effective precipitation anomalies following the methods described by Warken et al. (2024). For the analysis, the precipitation anomalies were aggregated using density-adaptive time bins, allowing temporal resolution to vary as a function of data density while avoiding over-segmentation in sparsely sampled intervals. Climatic regimes were identified using similarity-based segmentation of the adaptively binned anomaly series, with regime boundaries defined by locally elevated rates of change (local threshold $= mean(ts) + 2*SD(ts)$ across ts due to multiannual resolution and 5 year running mean). Mean anomaly values within each regime were classified as relatively wet or dry. The chronological periods from the archaeological records were overlaid and the binned values or derived means were extracted for each period. These were positively scaled to between 1 and 2 and serve as hydroclimatic index for the creation of the weighted friction models described below (Supplementary Fig. S2). The resulting index is applied as a single period-specific modifier of the terrain–hydrology friction surface. It is used to compare relative network configurations under wetter and drier phases, rather than to reconstruct climatic gradients within Hungary. This approach provides a common temporal hydroclimatic weighting across the archaeological periods, but it does not resolve local climatic variation within the study area. PastClim provides access to gridded palaeoclimate and bioclimatic reconstructions for specified regions and periods (Leonardi et al., 2023). Such spatially explicit information is not incorporated into the present friction model, which does not include a spatially varying palaeoclimate or agricultural-suitability component. The results should therefore be interpreted as comparative network configurations under period-specific hydroclimatic weighting, not as reconstructions of spatial climate conditions or agricultural potential across Hungary.

4.4. Least Cost Path estimates

Six chronological periods spanning from the Neolithic to the Hungarian Conquest period were subset from the dataframe provided in this analysis. Only complete cases with geographic information (Lat, Lon) and sufficient sample size of the original data inside the modern boundaries of Hungary were selected and reprojected to a meter-based coordinate system (EPSG:3857). Small subsets, for example labelled "Migration Period" were not considered practical for spatial analysis due to low sample size and ambiguous chronological classification. For formal analysis, we prepared a window of operation with a 100 km buffer around modern-day Hungary to avoid edge effects with points falling outside of the study area or being located at the margins (e.g. Wiegand and Moloney, 2004). Site intensities of each point pattern were calculated using a Kernel Density Estimate (KDE) function in the *spatstat* package (Baddeley et al., 2015) with a Gaussian bandwidth (sigma) of 2000 m and a grid cell size of 250 m, which captures local-scale intensities but preserves spatial separation between nearby centers. To delineate core areas, each KDE surface was capped using a value-based criterion using *mean* + 2**SD* of each KDE grid and subsequently set to binary rasters and then vectorized to polygons. We calculated centroids across each polygon to reduce the point pattern total number and to distinguish centers from scattered and noisy site distribution. This results in KDE-derived centers of 215 for the Neolithic period, Copper Age = 194, Bronze Age = 308, Iron Age = 292, Roman/Early Medieval period = 154, Hungarian Conquest period = 526 sites.

To evaluate the robustness of the KDE-derived network nodes, sensitivity analyses were performed for KDE bandwidth and threshold strength. KDE bandwidth values between 500 and 5000 m and threshold values between mean + 1 SD and mean + 3 SD were evaluated independently while holding the remaining parameters constant. Increasing KDE bandwidth progressively merged neighbouring archaeological concentrations and reduced the number of extracted network nodes, whereas smaller bandwidths produced increasingly fragmented node configurations. Similarly, low threshold values generated numerous weak density peaks and extensive archaeological footprints, whereas high thresholds retained only the strongest occupation concentrations. The selected parameter combination (sigma = 2000 m; threshold = mean + 2 SD) produced intermediate node numbers across all archaeological periods, while avoiding excessive fragmentation and spatial aggregation (see Supplementary Figs. S3–S4 and Supplementary Table S1).

To test overall connectivity of the samples, we ran Least Cost Path (LCP) (e.g. Verhagen et al., 2019; Herzog, 2014) analysis from each site to each center and from each center to each other center in the sample via the *rgrass* package (Bivand, 2023) and Tobler's hiking function (Bilotti et al., 2024; Kempf et al., 2025; Kempf and Denis, 2024; Tobler, 1993). Input friction in the model was calculated from minmax-normalized elevation (dem_norm) and simulated and normalized flow accumulation (flow_norm) generated from the *Rsagacmd* package (Pawley, 2023) and the *successive_flow_routing* algorithm on the elevation model with the same 100 km buffer to avoid forcing LCPs into a restricted window (friction = dem_norm + 2*flow_norm). From all lines, we sampled regular points at 1000 m distance and computed KDEs with a sigma of 1000 m and a cell size of 250 to produce high movement probability or movement intensity corridors between center-center and center-periphery of each valid subset. From each vector of single linestrings connecting all points in each subset, we calculated the travel time using a slope raster in radians based on the DEM and Tobler's hiking function from regularly sampled points at a spacing of 250 m along each linestring (Tobler speed = 6 * exp(-3.5 * abs(slope_radians + 0.05))). Based on travel time across each connection, we defined a network (MST, Minimal Spanning Tree) that connects all sites via the shortest travel time with optional two additional edges to increase complexity of the network but keep the potential connections at a minimum level. This produced a fully connected network between centers for each chronological subset based on terrain and hydrologic accessibility and permeability and serves as a baseline for the climatically weighted networks calculated for each period.

4.5. Climatically weighted networks

We applied a customized network approach using the GRASS implemented module *v.net.models* developed by Benjamin Ducke (Ducke and Suchowska, 2022). On Windows, *v.net.models* is implemented as a Bash script and is called via.bat launcher files. To enable robust use of the module via the *rgrass* interface, we applied system-level adjustments without modifying the module's core code or algorithm. To avoid issues with spaces in the default installation path, we created a directory symlink pointing to the GRASS installation and used this path as gisBase in R. We then adapted the GRASS batch wrappers for script-based modules (e.g. *v.net.models.bat*, *v.sort.bat*) so that they explicitly call the MSYS2 Bash shell (*sh.exe*) and correctly propagate GISBASE and MSYSPATH environment variables. This ensures that, when *v.net.models* is executed from R, all internally called GRASS scripts (used for preprocessing and attribute handling) are found and executed in the expected shell environment. No changes were made to the internal logic of *v.net.models*, only the Windows launcher configuration was adjusted so that the original GRASS script can be used directly from R.

We generated a complete network among all KDE-based thresholded sites using the above described friction model as a basis for a cost surface, in which each cell represents cost to travel through that cell (Conolly and Lake, 2006). The friction model was adapted to each chronological (archaeological) bin using the climate indices from hydroclimate reconstructions described above (Kempf et al., 2025). In addition, we applied a logarithmic (climate weighted power) transformation to the cost surface in order to disproportionately amplify high friction values associated with major river networks and high-elevation grid cells:

$$\text{friction} = \exp(\text{strength} * \text{weight} * \log(\text{friction} + eps))$$

in which friction is the composite raster of elevation and simulated runoff, *eps* is a small constant (1e-6) to avoid log(0), weight is the climatic index as positive scalar, strength (set to 1.5) is a tuning parameter to control how strongly climate can reshape the cost surface.

To evaluate the influence of climatic weighting on the friction surfaces, climate-weighting strengths between 0 and 2 and hydrological weighting factors between 0 and 3 were systematically tested. Mean, standard deviation, minimum, and maximum friction values were calculated for each period and parameter combination. Increasing climate-weighting strength resulted in smooth and monotonic reductions in mean friction values across all archaeological periods, indicating stable model behaviour without abrupt threshold effects. Similarly, increasing hydrological weighting produced gradual increases in friction values, particularly in areas characterized by elevated runoff accumulation. The parameterization (climate-weighting strength = 1.5; hydrological weighting = 2) produced intermediate friction conditions and avoided climatic overfitting and excessively amplified environmental barriers (Supplementary Figs. S5–S6).

The archaeological site coordinates were converted to simple point geometries and assigned unique integer IDs before being imported as a GRASS vector map. The *v.net.models* module requires consecutive numbering of input sites. We used the GRASS module *r.cost* in the R environment to generate a continuous accumulated cost surface from each archaeological subset. Knight's-move neighbourhood was applied for improved isotropy. Because *r.cost* assigned zero cost to starting locations, which caused subsequent network cost calculations to fail, resulting zero cost cells were replaced with a small positive constant

(0.01). From that, a complete network was calculated for each subset.

To derive a non-redundant representation of movement corridors, overlapping least-cost path networks were flattened using the *overline2()* function from the *stplanr* package (Lovelace and Ellison, 2019) in R. This approach aggregates coincident and partially overlapping line geometries into a set of unique corridor segments, while preserving information on the frequency with which individual paths contribute to each segment. The resulting attribute records the cumulative traffic density, defined as the number of overlapping least-cost paths supporting each corridor segment. For each segment, travel time was estimated using Tobler's hiking function as described above (Tobler, 1993).

4.6. Center-periphery models

To analyse how connectivity evolved across the cultural subsets, two complementary datasets were used for each period: (1) the center–-center network via the climatically weighted connections, and (2) a set of climatically weighted periphery–center connections representing travel from all sites to their two nearest computed centers using the LCP and MST approach described above (Kempf et al., 2025). This approach captures both the structure of inter-center networks and the accessibility of the surrounding hinterlands. Using the LCP estimates described earlier, we calculated the shortest travel time for each hinterland site to a subset of five nearest centers based on Euclidean distance. We selected the two shortest overall travel pathways for each site within each cultural subset, resulting in thousands of center-periphery connections across the entire temporal coverage. For each period, center–periphery metrics were computed by aggregating travel time values. (1) At the periphery level, the total number of periphery sites and their associated travel times allowed for the calculation of the following descriptive indicators: the mean and median travel time to the nearest center, the proportion of sites within 1 h of travel, and a measure of inequality in accessibility using the Gini coefficient (e.g. Gastwirth, 1972). (2) At the center level, each center was characterized by the number of periphery sites linked to it, along with summary statistics of these sites' travel times.

4.7. Site distribution density persistence

Spatial persistence across all periods was quantified by overlaying the dissolved KDE core areas (as polygons) from all periods. The union of all polygons was partitioned into non-overlapping spatial units, and for each unit the number of periods in which it occurred was counted (overlap). This yields a spatial persistence map in which the color code represents the number of chronological periods whose KDE cores include a given location. For each period, the total footprint area (km^2) was calculated, together with the proportion of the covered study region. Spatial persistence was summarised using the area-weighted mean overlap, representing the average number of overlapping periods within that period's footprint, weighted by the polygon area.

4.8. Ecozone/biome classification and archaeological footprint persistence

Ecozones/biomes were calculated for the extent of the Hungarian administrative boundary using the variables topography (elevation), temperature, and climatic moisture index (Depaermentier et al., 2025a, 2025b; Kempf, 2026a). These variables describe broad topographic, thermal and moisture gradients across the study area. The resulting classes are descriptive environmental groupings and do not represent a direct assessment of agricultural suitability, soil quality or crop productivity. Soil properties are relevant to cultivation and settlement but are not included as an independent variable in the present clustering. We applied K-means cluster analysis to create descriptive biomes using the approach presented in Kempf (2026). We tested for cluster stability using the silhouette method, elbow method, and gap statistics on a capped subset of 40% (max 10,000 cells) of the study area. Candidate K-values were estimated between 2 and 30 and silhouette scores were extracted. Silhouette K-means favours small K for most stable clusters and with continuous environmental data, plateaus develop at which no enhanced diversification between clusters is achieved. We added the within-cluster sum of squares (WSS) to assess the elbow point in variance reduction. Gap statistics were further applied to estimate cluster separation and marginal improvements were examined to detect plateau behaviour indicative of over-segmentation (K after the 1-SE rule = 4; K after 15% of max marginal gain using the elbow method = 5). Candidate K-values were then evaluated using bootstrap resampling (B = 30) to assess cluster stability via Jaccard similarity indices and $K = 6$ was selected as best representation of stability and interpretability with all clusters exceeding the stability threshold of 0.75 (<0.60 unstable cluster; 0.60-0.75 weak stability; 0.75-0.85 acceptable; >0.85 stable cluster) (Fig. 3; Table 1).

We then evaluated whether archaeological activity landscapes differed environmentally between periods using the spatial overlap between the KDE footprint polygons described above and the environmental biome classes. The KDE footprint polygons were intersected with the biome polygons, and we calculated the archaeological footprint surface areas for each biome. We normalized the biome coverage prior to statistical comparison because biome classes differ substantially in spatial extent across Hungary. The Pearson chi-square test of independence was applied to test whether environmental distributions differed between periods, following the null hypothesis that the biome composition of archaeological footprints is independent of chronological period.

4.9. Carbon and nitrogen stable isotope data

As one attempt to test whether shifts in settlement and land-use patterns can be associated with shifts in subsistence strategies over space and time, we collected published carbon (C) and nitrogen (N) stable isotope data (expressed as δ^{13}C and δ^{15}N in ‰) from the open access online repositories CIMA (Cocozza et al., 2022) and IsoArch (Salesse et al., 2018), from a recent large-scale study (Depaermentier et al., 2025a), and from further open access literature (Cavazzuti et al., 2025; Lazaridis et al., 2025; McCall et al., 2022). The data was subdivided into the same periods as defined from the archaeological dataset presented above (Depaermentier, 2026). We furthermore differentiated the δ^{13}C and δ^{15}N data derived from humans, from herbivores and from omnivores in order to specifically investigate human diet and husbandry practices (Lee-Thorp, 2008) and to get insights into potential ecological fluctuations (Depaermentier et al., 2025c). Based on the site location (i.e., longitude and latitude), each entry was moreover assigned to the respective ecozone cluster as defined from the model described above.

Scatterplots of human, herbivore and omnivore collagen isotope data were produced using the *ggplot2* (Wickham, 2016) package and R Software to visualize patterns in δ^{13}C and δ^{15}N data variability over time, while combined beeswarm and boxplots of human and herbivore collagen δ^{13}C and δ^{15}N data were produced using the *ggbeeswarm* package (Clarke et al., 2025) to observe such patterns among ecozone clusters. The latter selection is based on the fact that the isotopic composition of herbivore tissues directly derives from the ingested plants, i.e. from a less diverse diet than omnivore mammals – including humans. Herbivore δ^{13}C and δ^{15}N values are therefore considered to be more likely affected than omnivores by both potential husbandry practices and local environmental and climatic conditions. Their isotopic composition thus provides a robust comparison to the human dataset when investigating the potential influence of environmental and climatic conditions on the measured δ^{13}C and δ^{15}N values. We used ANOVA-tests based on categorical variables (from the periods and the ecozones) to verify whether the carbon and nitrogen isotope values of humans and herbivores statistically significantly differ among groups, i.

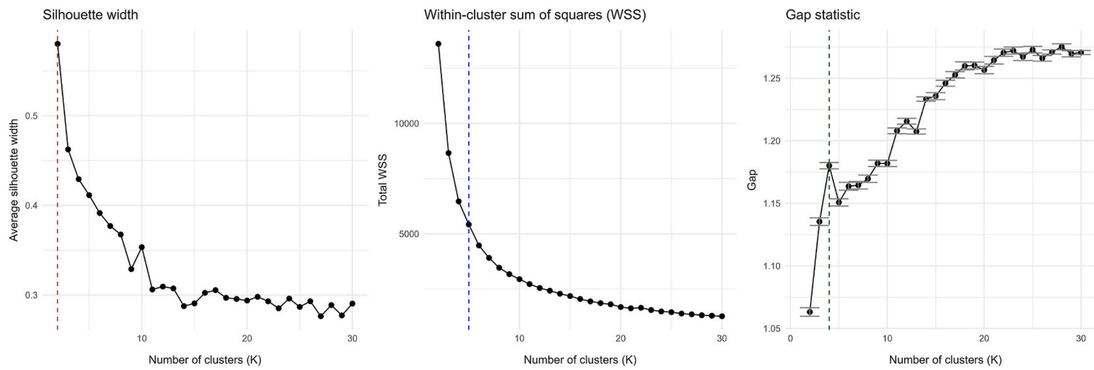

Fig. 3. K-means cluster stability test results for Hungarian ecozone clusters using silhouette method, WSS elbow method, and gap statistics. The y-axis units are: average silhouette width (dimensionless): a normalized index describing how well each observation fits its assigned cluster compared to the nearest alternative cluster (1 = points are very well separated from other clusters; 0 = cluster overlap; <0 = potentially wrong cluster assignment); total within-cluster sum of squared distances (dimensionless): the total squared distance between each observation and the center of its assigned cluster; gap statistics (dimensionless): the difference between the clustering compactness observed in the data and that expected from randomly distributed data. The dashed lines are model-selected silhouette $K = 2$, WSS $K = 5$ and gap $K = 4$.

Table 1
K-means cluster stability test results for Hungarian ecozone clusters using silhouette method, WSS elbow method, gap statistics, and Jaccard similarity indices (mean and minimum values given as mean values can hide bad clusters; PCLstab≥0.75 is the proportion of clusters whose stability ≥0.75) (cluster candidate $K > 1$).

Candidate K	Sil Scores	WSS	gap	SE	Mean Jaccard	Min Jaccard	PCLstab≥0.75
2	0.580	13602.4	1.063	0.003416	0.990	0.984	1
3	0.462	8656.7	1.135	0.003051	0.974	0.963	1
4	0.429	6468.9	1.180	0.002504	0.969	0.940	1
5	0.411	5425.2	1.151	0.002887	0.862	0.780	1
6	0.391	4473.9	1.164	0.003133	0.892	0.838	1
7	0.377	3912.4	1.164	0.003014	0.779	0.582	0.7143
8	0.368	3463.8	1.170	0.002896	0.858	0.747	0.8750
9	0.329	3174.8	1.182	0.002521	0.774	0.518	0.6667
10	0.353	2948.7	1.182	0.002463	0.831	0.766	1
11	0.306	2725.0	1.208	0.002314	0.658	0.313	0.2727
12	0.309	2547.5	1.216	0.002322	0.704	0.416	0.5000
13	0.307	2425.9	1.207	0.002051	0.833	0.748	0.9231
14	0.288	2288.7	1.233	0.001752	0.730	0.395	0.5714
15	0.291	2182.8	1.236	0.002794	0.734	0.438	0.5333
16	0.302	2050.8	1.246	0.002397	0.752	0.602	0.4375
17	0.305	1941.8	1.253	0.002540	0.789	0.588	0.5882
18	0.297	1862.6	1.260	0.003245	0.758	0.520	0.5000
19	0.296	1811.5	1.260	0.002708	0.755	0.506	0.6316
20	0.294	1686.7	1.257	0.002944	0.682	0.338	0.4000
21	0.298	1628.3	1.264	0.003038	0.723	0.571	0.4762
22	0.293	1652.5	1.270	0.002881	0.732	0.338	0.5455
23	0.285	1550.6	1.272	0.002815	0.685	0.441	0.3913
24	0.296	1485.3	1.267	0.002959	0.667	0.432	0.3333
25	0.287	1454.3	1.273	0.002609	0.651	0.459	0.2400
26	0.293	1390.3	1.266	0.002269	0.632	0.351	0.1923
27	0.276	1357.3	1.271	0.001670	0.678	0.424	0.2222
28	0.289	1314.5	1.275	0.002427	0.632	0.423	0.2143
29	0.277	1293.6	1.270	0.002475	0.645	0.400	0.1724
30	0.290	1268.6	1.271	0.001636	0.651	0.372	0.2333

e. among periods, among ecozones, and among ecozones within each period. We then applied Generalized Additive Models (GAM) to estimate which predictors explain the most patterns and variance of human and herbivore δ^{13}C and δ^{15}N values. For the GAM, we used numerical variables, i.e. the mean date for the temporal aspect, the longitude and latitude for the spatial aspect, and the mean TMP, mean CMI and mean ELV for the ecozone associated with each entry. In both cases, we ran the ANOVA tests and the GAM twice: first without accounting for the fact that individuals and animals are mostly grouped by site, and then accounting for the effect of this grouping by site. The related R-code is available from Depaermentier (2026).

5. Results and discussion

5.1. Site distribution intensities

Site distribution intensities and persistence in the Carpathian Basin are shown in Fig. 4, highlighting the chronological overlap of KDE centers from the Neolithic to the Hungarian Conquest period. The Neolithic and the Hungarian Conquest period show lowest overall impact on footprint size patterns, whereas Bronze Age and the Roman/Early Medieval period site densities contribute most. The Roman/Early Medieval period has maximum impact on site persistence patterns, followed by Copper Age and Neolithic sites. Spatially, the southern Tisza region shows strongest archaeological site densities across all periods, which is consistent with land-use potential and high-quality soil distribution but also with scientific biases caused by research interest and

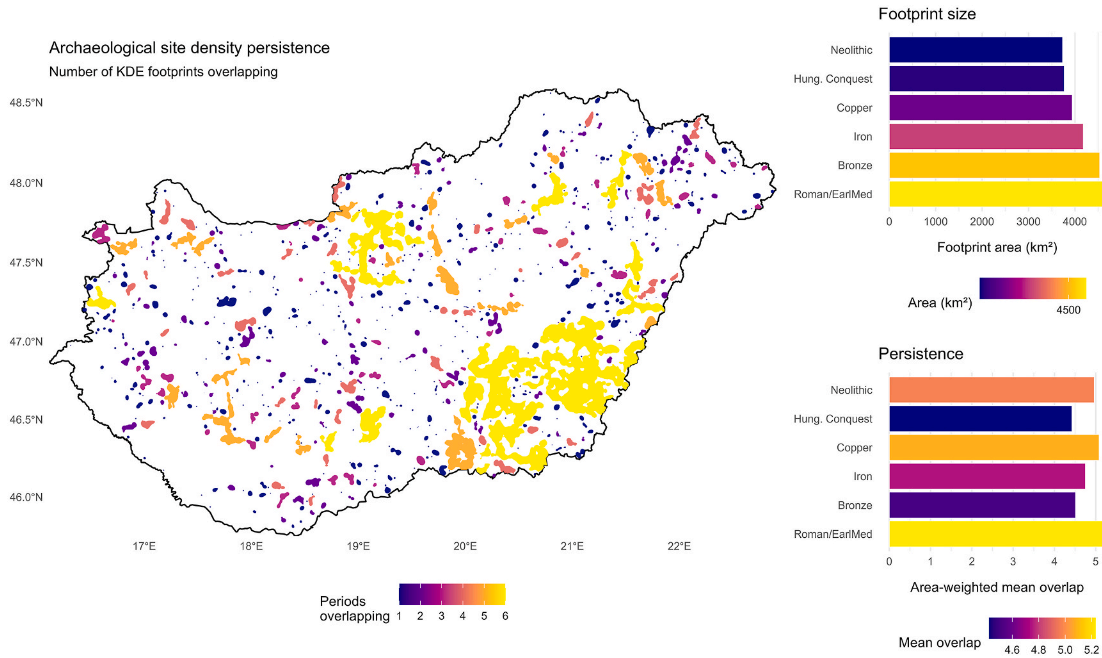

Fig. 4. Spatial persistence of archaeological site densities in the Carpathian Basin. Color values represent the number of archaeological periods whose KDE footprints overlap each location. High values indicate long-term persistence across multiple periods rather than dominance by any single phase. Roman/Early Medieval (Roman/EarlMed) and Bronze Age site intensity contribute most to the persistence patterns, whereas Neolithic and Hungarian Conquest period records contribute less in footprint size. The Roman/Early Medieval archaeological record spatially contributes strongly to site persistence in the southern Tisza region and at the northern Danube. (For interpretation of the references to colour in this figure legend, the reader is referred to the Web version of this article.)

sampling intensity (Kempf, 2021). High-persistence areas therefore represent locations where multiple archaeological periods coincide spatially, indicating repeated occupation across long temporal sequences or scientific bias rather than dominance by any single phase. The sensitivity analyses further demonstrate that the major archaeological structures identified by the KDE approach are remarkably robust to changes in parameterization. Although center numbers vary substantially with bandwidth and threshold selection, the overall spatial footprint of occupation remains comparatively stable through time, despite large differences in archaeological sample size. This suggests that the principal central structures identified by the KDE approach reflect persistent spatial organization within the archaeological record rather than artifacts of individual parameter choices and that the selected parameterization represents a stable intermediate solution that minimizes both over-fragmentation and excessive smoothings (Supplementary Figs. S3–S4, Supplementary Table S1).

5.2. Climate-adaptive networks for the Carpathian basin

Climatically weighted networks for center-center connectivity patterns were produced for each archaeological period using the custom friction model and a hydroclimatic wetness/dryness index based on the reconstruction presented in Warken et al. (2024), from which distinct communication networks were obtained for each period in the Carpathian Basin (Fig. 5). Sensitivity analyses demonstrate that both climate-weighting strength and hydrological weighting produced gradual and monotonic changes in friction values. No abrupt threshold behaviour or unstable responses were observed, indicating that the friction models are robust to moderate parameter variation. The gradual response of the friction models suggests that hydroclimatic conditions acted primarily as a modifying influence on landscape accessibility rather than as a deterministic control on movement behaviour. Environmental variability therefore likely altered the relative attractiveness of particular movement corridors while maintaining the broader structure of the regional connectivity (Supplementary Figs. S5–S6.

Increasing climate-weighting strength progressively reduced mean friction values across all archaeological periods, without abrupt threshold behaviour within the tested parameter range. This analysis evaluates the response of the friction surface itself. It does not independently test the stability of individual network edges, corridor configurations or centre–periphery indicators under alternative parameter settings. At higher climate-weighting values, the response curves flattened substantially, indicating smaller effects of additional weighting. Hydrological weighting produced a gradual and approximately linear increase in friction values. The selected hydrological weighting value represents an intermediate parameterization that balances riverine influences without dominating the friction surfaces.

This results in different responses to climate variability over the Holocene and the connection of socio-cultural centers and hubs via persistent routes and pathways. Because this study uses a spatially limited archaeological dataset, remote areas show less influence on the central connectivity than centers located in the central part of present-day Hungary.

The Neolithic connectivity patterns are preferably located on flat terrain outside the floodplains (Fig. 5), which accounts for the increased run-off variability, impacted by humid conditions during the early ($i = 1.884$) and late Neolithic ($i = 1.732$) compared to the slightly below average middle Neolithic period ($i = 1.407$). Major centers during the Neolithic are scattered across the study area with concentrations in Transdanubia in the west and Alföld in the east. These two centers are settled by differing archaeological cultures during the Neolithic, with trajectories from Starčevo to Transdanubian-LBK (Linearbandkeramik) in the west and Körös to Alföld-LBK in the east (Banffy, 2008; Banffy and Sümegi, 2012). While both groups had broadly similar lifestyles, their differing material substrates (decorated pottery, lithic networks) coincide with genetic differences, specifically more hunter-gatherer ancestry in the east (Gelabert et al., 2024). In contrast, the central part of modern Hungary, characterized by the Danube-Tisza Interfluve (DTI), has a particularly low site and network density. Because the DTI mostly consists of sandy land and salt-affected soils (Pásztor et al., 2018), this area was not particularly suitable for the early forms of agricultural exploitation, which likely explains why Neolithic sites are lacking there

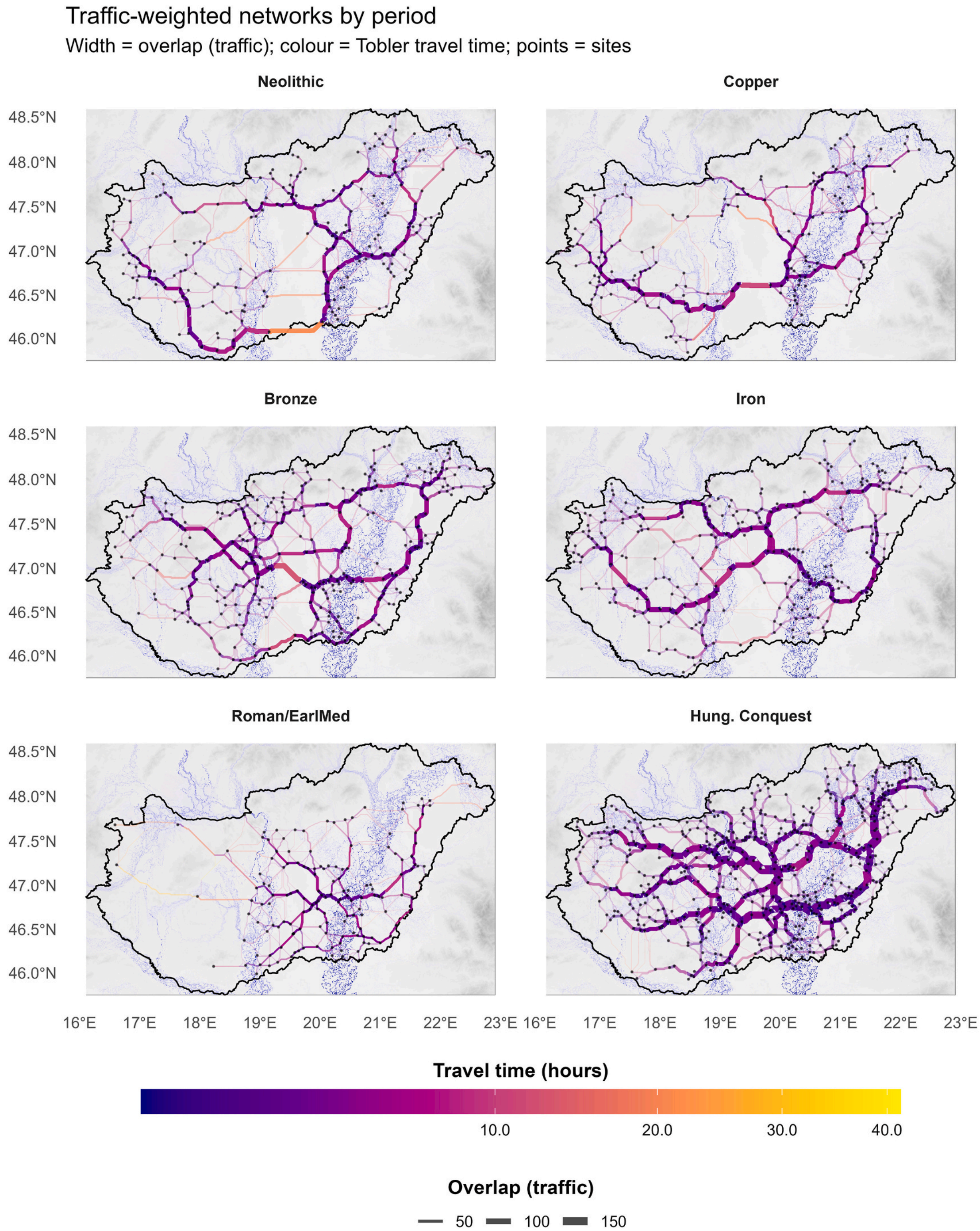

Fig. 5. Movement networks by period showing cumulative corridor use and travel cost. Line width shows the number of overlapping paths (traffic density), colour represents Tobler-based travel time (hours) derived from the slope of the accumulative cost surface and climatic weights for each period. Black points indicate center hubs derived from density estimates of all sites. (For interpretation of the references to colour in this figure legend, the reader is referred to the Web version of this article.)

(Banffy, 2013; Kempf, 2021). The south-north stretching network along the Tisza is most prominent and connects the southern hotspots of the early Neolithic Starčevo and Körös culture with the northern LBK cultural expansion (Jakucs et al., 2016; Oross et al., 2023). A southern high traffic connection is revealed by the model that connects the southern Tisza region with the western Transdanubian part. This reflects largely the westward spread of the Neolithic lifestyle in the Carpathian Basin (Banffy and Sümegi, 2012; Oross and Bánffy, 2009). In particular, the dominant south-north-orientation of Neolithic networks (Fig. 5) reflects the role of the Carpathian Basin as key transition corridor that facilitated the spread of Neolithic farming communities from the Balkans to the rest of Europe (Bánffy, 2019; Depaermentier et al., 2020a,b; Gaudenyi and Mihajlović, 2022; Gelabert et al., 2024; Lipson et al., 2017). During the Copper Age (average $i = 1.748$), the hydroclimatic conditions were rather humid with consistent values above average (early to late Copper Age: $i = 1.852$; $i = 2$; $i = 1.40$). The east-west stretching connections developed much stronger with the Transdanubian western part being integrated into the south-north network via the southern DTI (Fig. 5). With the onset of metal production, the important reliance on mineral (copper) sources had a decisive impact on long-distance and specialised networks (Gyucha et al., 2024), which built on pre-existing infrastructures and connectivities inherited from the Neolithic (Fig. 5). The Tisza river networks now stretch closely along the eastern and western margin of the extensive floodplain, avoiding high traffic river crossings and focusing on southern and less frequently used northern connections. The riverbed of the Tisza was highly dynamic in the early and middle Holocene with frequently changing channel locations following avulsion events that caused extensive flooding (Kempf, 2020; Kiss et al., 2014; Knipl and Sümegi, 2012). During periods of enhanced rainfall in the eastern Carpathian Mountains, these events would have significantly altered the riverbed characteristic, making the area vulnerable for settlement locations and enhancing the risk for agricultural production.

The Bronze Age (average $i = 1.27$) archaeological density shows an increase in center distribution along the river Danube and the northern and eastern part of Hungary, which affects the network model simulation and alters the connections between the central hubs (Fig. 5). The eastern river Tisza network gets more important as a major communication artery as well as more frequent east-west connections crossing the DTI and reaching Lake Balaton and Transdanubia. A small-scale network hotspot is visible in central Hungary, highlighting the importance of the river Danube compared to the marginal centers at that time, which coincides with more stable and drier climatic conditions (early to late Bronze Age: $i = 1.316$; $i = 1.298$; $i = 1.193$). This confirms the results of previous studies that put the increasingly important river-based-networks in perspective with their role in facilitating access to metal resources (Duffy, 2020) and to long-distance trading routes that developed during the Bronze Age (O'Shea, 2011), in parallel to significant socio-cultural developments (Kulcsár and Szeverényi, 2013). The marked east-west orientation of the networks further mirrors the intensified connectivities with and cultural influences from the East, as also attested by movement of populations across western Eurasia

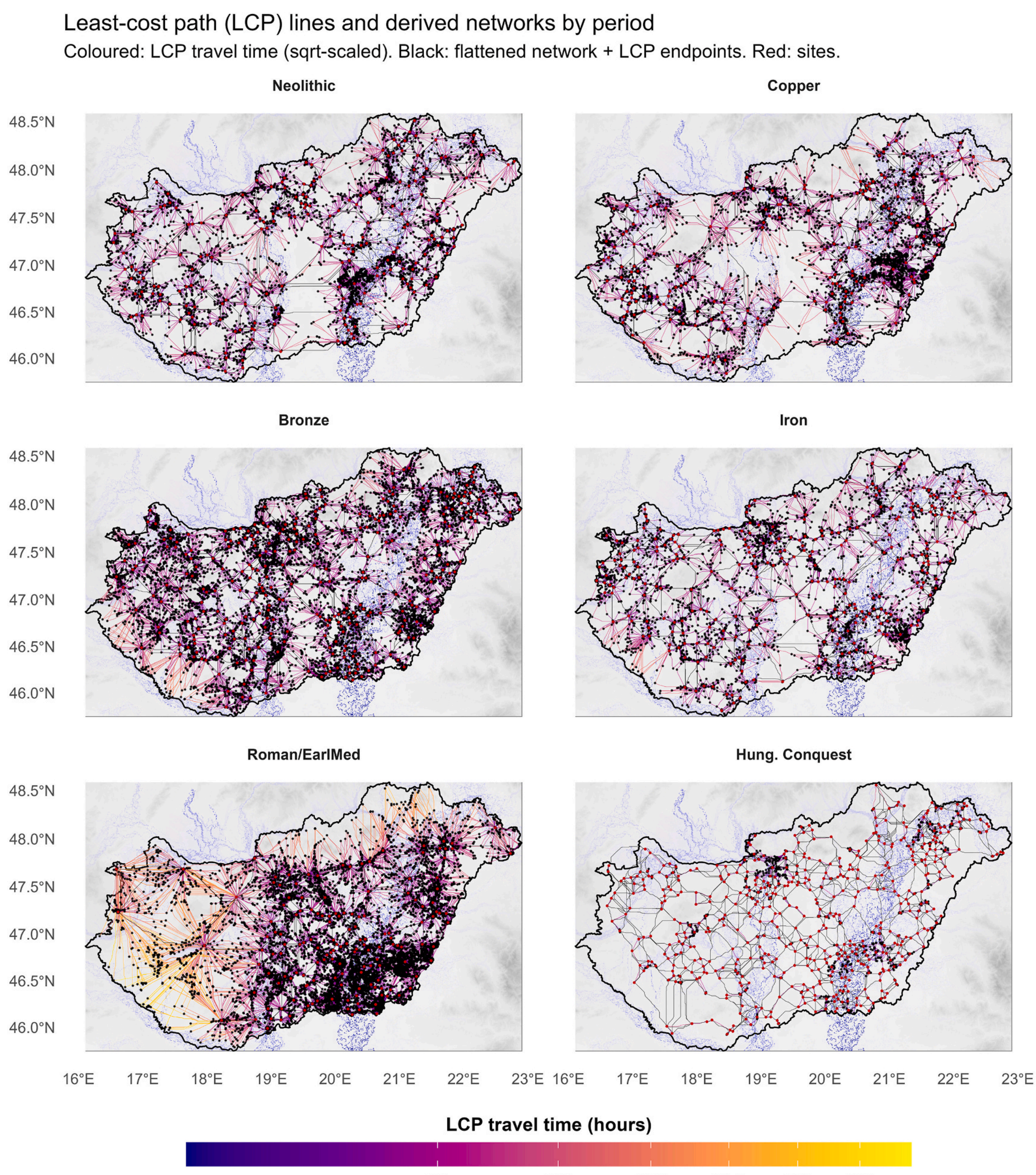

Fig. 6. Periphery-center networks with best connecting centers for each periphery site. Colour represents Tobler-based LCP travel time (hours) derived from the slope of the accumulative cost surface and climatic weights for each period. Centers are given in red, periphery sites are black dots. The black line is the flattened center-center network for each period. (For interpretation of the references to colour in this figure legend, the reader is referred to the Web version of this article.)

(Allentoft et al., 2015; Haak et al., 2015; Lazaridis et al., 2025).

This changed during the Iron Age ($i = 1$), where the DTI became a major hub in connecting the west with the east and the north with the south (Fig. 5). The rivers played a lesser role in the east-west connectivity patterns, however, drier conditions allowed for more frequent crossings and small-scale connections in east-west directions compared to north-south/south-north oriented networks. This result reflects the archaeologically attested intensification of east-west connections (Kemenczei, 2003) which took place in the framework of an unprecedented urbanization process associated with infrastructure developments (Fernández-Götz, 2018). The results of this network model, however, does not exemplify the increasing connectivity to the Mediterranean world.

In the Roman to Early Medieval period ($i = 1.163$), drier conditions prevailed initially followed by higher variability and pronounced phases of cooling, warming, and changes in hydroclimatic conditions (Büntgen et al., 2016; Luterbacher et al., 2016; Xoplaki et al., 2021). The central networks changed drastically with high density cores in the south-eastern Carpathian Basin and the river Tisza region (Fig. 5). The communication intensity is reduced despite a strong increase in site numbers, mirroring the more dispersed and scattered peripheral occupation during this period (Fig. 6). The core density central hubs dominate the dispersal and account for strong influence of the southern Hungarian region compared to the northern and western parts. The dominating clusters result in lesser numbers of central hubs and hence lesser large-scale communication, which strongly increases the travel time from the periphery to the centers, particularly in the western part of Hungary. The overall mean travel time is high, the share of the periphery to the centers within 1 h is the smallest across all periods, which reduces the Gini equality index drastically (Fig. 7).

This result contrasts with the expectations of intensive long-distance connectivities during this period, characterized by the gradual integration of the Carpathian Basin (i.e. Pannonia) into the Roman Empire and its widespread, sophisticated and multifaceted infrastructures (Dermody et al., 2014; Scheidel, 2015), followed by the so-called Migration Period and expansion of various kingdoms throughout the period (Alt et al., 2014; Amorim et al., 2018; Halsall, 2014; Maróti et al., 2022). During the Hungarian Conquest period, the climatic conditions were relatively humid, which would further influence the development of transportation and movement corridors close to the river beds and control also selective crossings ($i = 1.903$). The archaeological site distribution changed accordingly, and much more dispersed patterns led to an increased number of dominating clusters compared to smaller total number of observations. This is pushing the traffic intensity to more long-distance communication based on short-interval connections spanning most of modern-day Hungary (Fig. 5). East-West communication is strongly expressed stretching towards the margins of the operational window. Due to the dispersed site distribution, the mean travel time from peripheral site to next center is small (Fig. 7) because most dispersed sites form a center itself. Only two larger site concentrations can be observed, in the southern Tisza region and around Budapest, which slightly influence the center-periphery connectivities.

5.3. Environmental preferences and land-use strategies

An ecological zonation has been computed to identify similarity clusters of environmental factors that contribute to land-use strategies, settlement distribution and network development in the Carpathian Basin. The unsupervised, deterministic K-mean algorithm was used with a stability-tested $K = 6$ on elevation (ELV), temperature (TMP), and climatic moisture index (CMI), resulting in six distinct biomes (Fig. 8 upper panel). There is a strong gradual trend in ecozone development starting from the south-eastern lowlands of the lower Tisza floodplain region that is characterized by highest annual average temperature and the overall lowest moisture availability. Towards the margins of the basin, temperature declines with higher elevation. Moisture availability increases and is highest in the Carpathian Mountain ranges in the northern part of modern-day Hungary.

Spatially, the ecozone with highest TMP and lowest CMI in low-lying floodplains dominate the cluster results (Fig. 8, middle panel), however, the normalized footprint comparison shows that the Neolithic, Bronze Age, Copper Age and particularly the Roman/Early Medieval high intensity core areas are strongly distributed across the plains of the south-eastern Tisza river system. These floodplains and meadows are also highly fertile with meadow Chernozems and fluvisols frequently abundant in soil mosaics (e.g. Pásztor et al., 2018), potentially increasing

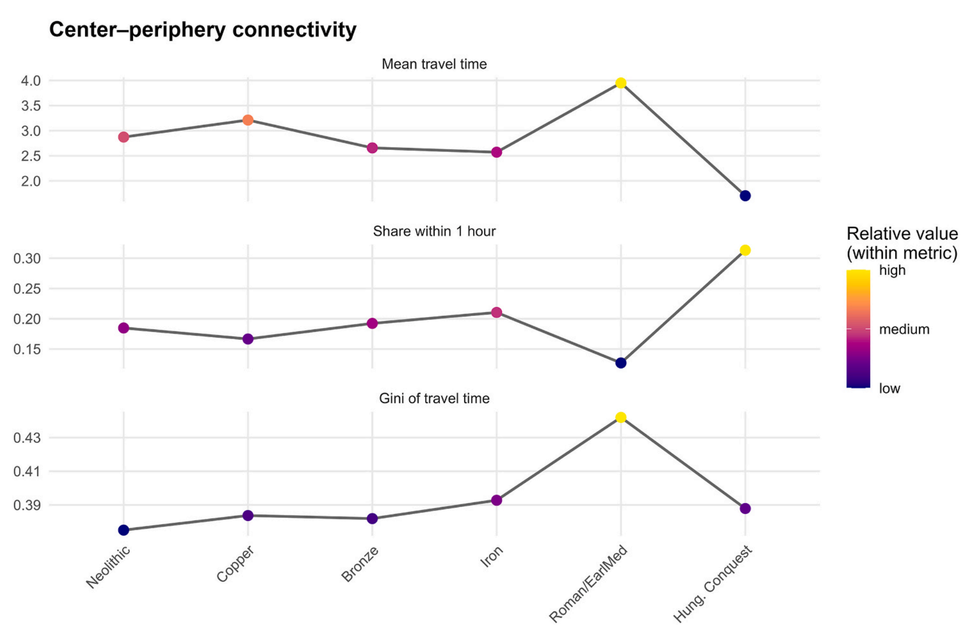

Fig. 7. Center-periphery connectivity for the archaeological periods based on the least-cost derived connections of the two nearest centers for each peripheral site. Travel time is given in mean (hours) (upper panel), share within 1-h travel time (middle panel), and Gini index of travel time, indicating equality (towards 0) or inequality (towards 1). The Roman/Early Medieval period has the highest inequality among center-periphery connectivity, highest mean travel time and lowest share within 1 h of travel.

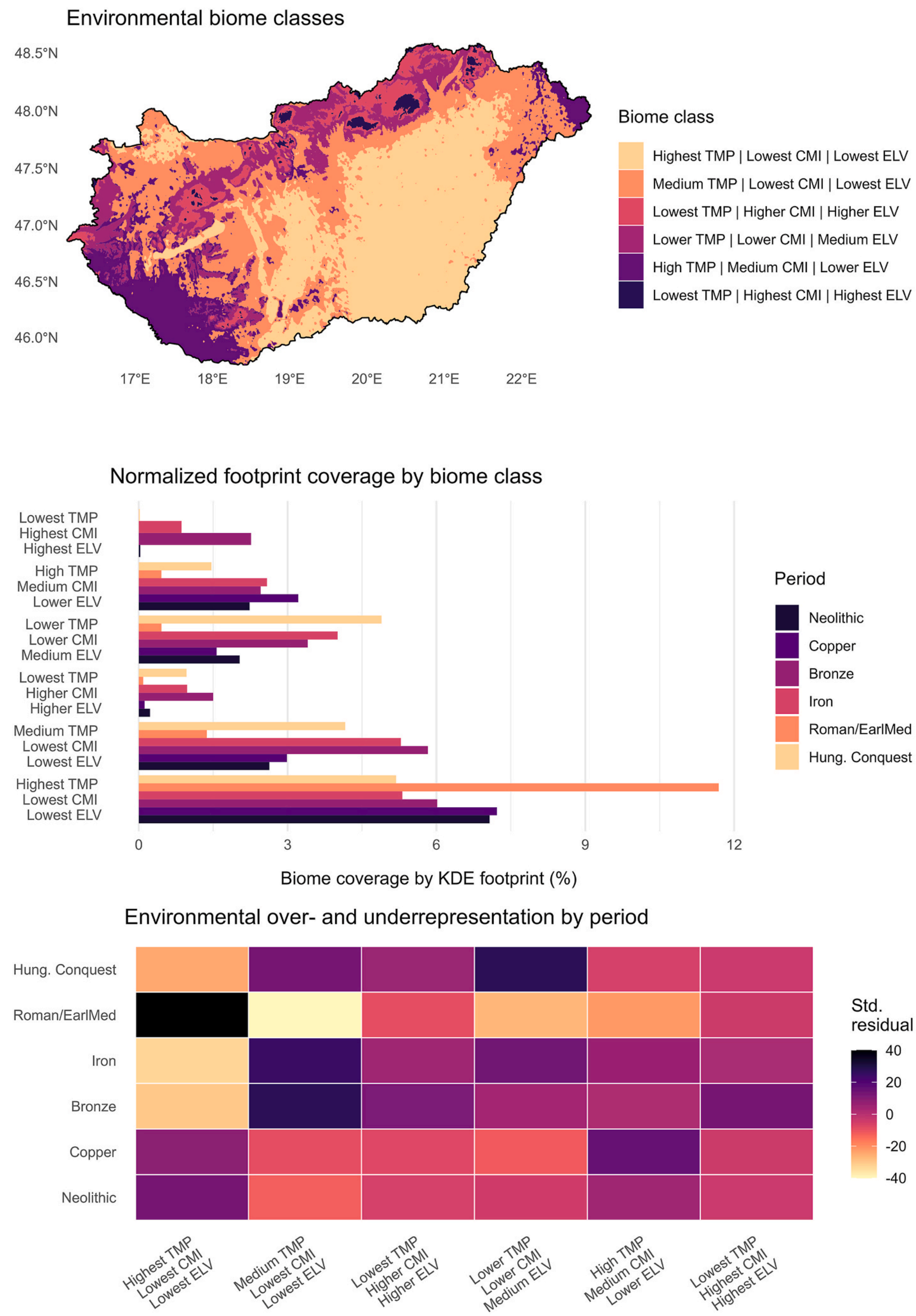

Fig. 8. Environmental distribution of archaeological landscape footprints across biome classes. Upper panel: Environmental biomes in Hungary from unsupervised *K*-means cluster analysis (stable $K = 6$) of elevation (ELV), temperature (TMP), and climatic water balance (CMI) (Kempf, 2026). Middle panel: Distribution of archaeological clusters across ecological biomes. Bars show the percentage of each biome class covered by the archaeological footprint for each chronological period (KDE). The coverage was normalized by the total biome area to indicate relative environmental representation. Lower panel: Standardized residuals from the chi-square test of independence between period and biome class. Positive residuals indicate environmental zones that are more strongly represented than expected for a given period, while negative residuals indicate underrepresentation (residuals were truncated to improve visual comparability across cells).

agricultural exploitation during prehistory. Loess-soil based land-use during the Neolithic period, however, is still highly debated and multiple hypotheses link prehistoric forest clearance, landscape transformations, and land-use to the development of Chernozems from hydromorphic loess-soils or luvisols (e.g. Strouhalová et al., 2020; Kempf, 2021; Lehmkuhl et al., 2021; Magyari et al., 2024). This debate also relates to the older "steppe theory", according to which early farming in Central Europe may have started in areas that were not completely forested but retained remnants of natural steppe or forest-steppe vegetation from the Late Glacial/Early Holocene (Pokorný et al., 2015). The floodplain of the river Tisza, in general, provides a wide range of fertile soils, freshwater availability, making it highly suitable for agriculture and animal husbandry. How these landscapes were impacted by climatic conditions, particularly during the growing season, is further debated. Betti et al. (2020) showed that major slowdowns in the spread of farming across Europe coincided with climatic thresholds affecting growing-season conditions, suggesting that climate primarily acted through agricultural suitability and resource availability rather than through direct deterministic forcing. In this sense, climate should be understood as one factor operating within broader socio-ecological resilience dynamics, in which Early Neolithic communities could respond to environmental stress through adaptation, reorganisation, mobility, or changing interaction with hunter-gatherer groups (Gronenborn et al., 2014). Recent high-resolution palaeoenvironmental evidence from Santovka, Slovakia, provides a local-scale example of such environmentally dynamic settings, showing that regional hydroclimatic variability coincided with hydrological instability, lake-level changes, and ecological reorganisation during the Mesolithic–Neolithic transition and the Early Neolithic period (Petřík et al., 2026 in preparation).

This ecozone cluster is over-represented relative to its spatial extent during the Neolithic period, the Copper Age, and the Roman/Early medieval period (Fig. 8, lower panel). In contrast, the widely distributed Bronze Age sites show rather repulsion for this ecozone, and instead a preference for the medium temperature cluster surrounding the south-eastern Carpathian Basin, avoiding the extensive high temperature floodplains during a period of increasingly dry conditions. This land-use shift is associated with a sudden increase in human collagen δ^{13}C values above −18.0‰ in the Bronze Age (Fig. 9), which can be considered a robust isotopic indicator for millet consumption in this region (Depaermentier et al., 2025b). This correlated with isotopic and archaeobotanical evidence for the arrival of millet in Central Europe (Cavazzuti et al., 2025; Filipović et al., 2020; McCall et al., 2022). With its specific properties including a resistance to drought, salinity and poor soil conditions, millet was an ideal crop to cope with extreme conditions attested for this period (Dreslerová et al., 2013, 2017), and land-use shifts associated with millet arrival are attested in other regions of Europe as well (Orfanou et al., 2026; Depaermentier et al., in preparation). Millet resistance to water scarcity and saline soils, can also be linked to soil conditions in the Carpathian Basin. The Danube-Tisza-Interfluve and large parts of Central and northern Hungary exhibit salt-affected soils (Pásztor et al., 2018), which impact the local vegetation (Tóth, 2010) but were also an important part of animal husbandry (Bánffy, 2015).

Not enough animal data is available to draw reliable conclusions from isotopic data on related shifts in husbandry practices (Fig. 9). However, the very specific distribution of Bronze Age and Iron Age sites over ecozones that were otherwise neglected during previous and subsequent periods may furthermore mirror the evolution towards a mixed farming or agro-pastoralist economies that characterized those periods (Bartosiewicz, 2003; Chapman et al., 2009; Kemenczei, 2003; McCall et al., 2022). The Bronze Age is moreover marked by major social, economic, and technological transformations, including the widespread adoption of bronze metallurgy, increasing social stratification, long-distance exchange networks, and the formation of complex settlement hierarchy, and the rapid spread of millet across Europe (Cavazzuti et al., 2025; Filipović et al., 2020). Due to its short vegetation period and low requirements in the cultivation process, millet (as identified from elevated δ^{13}C values on Fig. 9) was particularly well adapted to these subsistence economies that implied a great degree of mobility (Dreslerová et al., 2013, 2017; Miller et al., 2016). It can be stressed that millet remained a particularly important component of human diet from

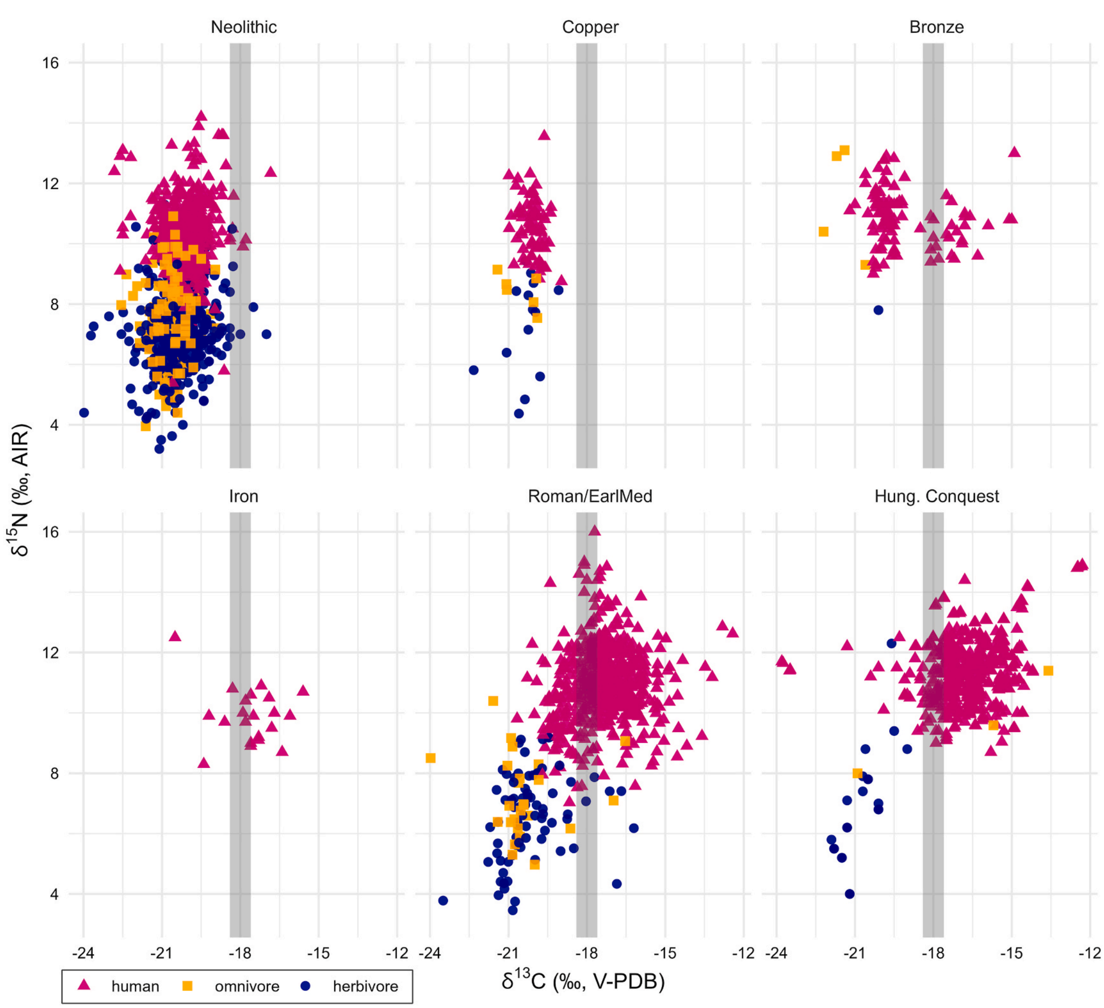

Fig. 9. Diachronic evolution of the δ^{13}C and δ^{15}N from human and animal remains in the Carpathian Basin. The grey shaded area around −18.0‰ represents the commonly accepted δ^{13}C threshold value to distinguish a C_3 diet (below −18.0‰) from a diet including C_4 food such as millet (Depaermentier et al., 2025b). Detailed results of the ANOVA tests verifying the significance of δ^{13}C and δ^{15}N fluctuations over time for humans and herbivores are in Table S2.

the Bronze Age to the Hungarian Conquest Period in the Carpathian Basin (Fig. 9). In a similar way as for the Bronze and Iron Age agro-pastoralist communities, this has been also explained by the suitability of a crop with short vegetation period for highly mobile groups during the Early Middle Ages (Alt et al., 2014; Amorim et al., 2018; Hakenbeck et al., 2017; Knipper et al., 2020) and as response to challenging environmental conditions in the later medieval phase (Gugora et al., 2021). Elevated areas with lowest temperatures and increased precipitation are less frequently utilized and remain only randomly occupied compared to their spatial availability (Fig. 8, lower panel). Normalized biome coverage indicates that archaeological landscape footprints were not evenly distributed across environmental classes (Fig. 8, middle panel). This pattern is confirmed by the chi-square residual heatmap (Fig. 8, lower panel), which identifies distinct period-specific overrepresentation in particular biome types.

In contrast to human δ^{13}C, the available animal data do not show a comparably clear temporal shift (Fig. 9; Table S2). Because animal observations are limited and unevenly distributed, they cannot provide a robust basis for evaluating changes in husbandry practices through time. However, this difference in temporal pattern suggests that the shift in human data is triggered by changes in subsistence practices. But given the ecological diversity attested across Hungary and the different use of those ecological clusters over time (Fig. 8), it remains key to assess the role of ecological diversity on carbon and nitrogen isotope variability (van Klinken et al., 2002; Depaermentier et al., 2025b, 2025c) in order to disentangle anthropogenic and environmental drivers (Depaermentier et al., 2025a). The expected trend for the highest collagen δ^{13}C and δ^{15}N within the ecozone cluster "Highest TMP | Lowest CMI | Lowest ELV" and the lowest values within the ecozone cluster "Lowest TMP | Higher CMI | Higher ELV" is only observed among human data (Fig. S7a–b), whereas herbivores neither vary much nor reflect expected trends (Fig. S7c–d). If not accounting for the effect of the site to which humans and animals are assigned, the pairwise and combined ANOVA tests reveal statistically significant differences among periods, ecozones and ecozones within each period for both δ^{13}C and δ^{15}N data in human remains (with all p-values ≤ 7.4e-11) and among ecozones for δ^{13}C (p-value: 0.04) and δ^{15}N (p-value: 0.0001) data in herbivore remains (Table S2). But when accounting for the site-affiliation effect, only the period-only-test on human δ^{13}C shows significant results (p-value: $<$2.2e-16; while all other tests show p-values above 0.07).

The GAM approach then confirmed that human collagen δ^{13}C is not explained by ecology alone and revealed that the chronological pattern dominates, while ecological/environmental variables provide substantial additional explanatory power (Table S3, Fig. S7a). This result applies both with and without accounting for the site effect, with the model explaining respectively 76% and 71% of the variance, and the mean date (CE/BCE) being the most (or only) significant predictor (p-value $<$ 2e-16). Similar results are obtained for human collagen δ^{15}N data yet with less robust models (up to 46% of the variance explained), while animal data produce no strong or significant results (Table S3). This suggests that the observed shifts in isotopic data – in particular the increase in human collagen δ^{13}C from the Bronze Age – is not a direct effect of the different ecological settings in the settled areas, but of a change in subsistence practices such as the adoption of millet. Yet it remains plausible that the adoption of millet was triggered by or enabled the land-use shift observed from the archaeological records (Fig. 8).

6. Conclusions

This study provides a standardized and replicable framework for diachronic comparison of archaeological connectivity patterns in the Carpathian Basin dating from the Neolithic to the Hungarian Conquest period by combining site-density derived centers of, climatically adjusted least-cost movement simulations, center–periphery analysis, ecological zonation, and stable isotope evidence from human and animal remains. Using a custom-tailored network analysis, we present a new method to assess cross-chronological communication structures, settlement center hierarchies, and land-use patterns across archaeological periods and diverse palaeoenvironmental settings.

Our results show that communication and connectivity patterns in the Carpathian Basin were highly dynamic across space and time. Areas of long-term archaeological persistence, especially in the southern river Tisza floodplain region, are most likely connected to the recurrent importance of particularly favourable parts of the landscape, for example for agricultural production and animal husbandry. At the same time, the organization of central hubs, the accessibility of the associated hinterland and the complementary region, and the degree inequality associated with center–periphery connectivity changed substantially across the chronological phases considered here, showing that long-term spatial persistence coexisted with repeated reconfiguration of communication structures. One central outcome of the analysis is that archaeological site abundance alone is not a sufficient indicator of regional integration. The center–periphery comparison shows that accessibility was unevenly distributed across all periods, but to different degrees. The Roman and Early Medieval period in particular stands out for the highest inequality, the highest mean travel times, and the lowest share of peripheral sites located within 1 h of a centre compared to all other periods. By contrast, more dispersed site distributions generated a larger number of local centers and shorter travel times between peripheral sites and their nearest hubs. One of the main lessons from this comparison is therefore that densely occupied landscapes did not necessarily form the most evenly integrated communication systems.

The ecological and isotopic comparison data add an important second dimension to these hypotheses. Archaeological footprints were not evenly distributed across the biome classes calculated for the Carpathian Basin, and these associations changed through time. The Neolithic period, Copper Age, and Roman and Early Medieval core areas are strongly linked to the south-eastern lowland biome of the Tisza system, characterized by the highest annual average temperature and the lowest climatic water balance within the study area - a region that is more vulnerable to prolonged droughts during periods of hydroclimatic instability. The Bronze Age site distributions show a different ecological configuration and avoid the extensive high-temperature floodplains. The isotope evidence is consistent with this shift, indicating the increasing importance of millet agriculture from the Bronze Age onward and its continued relevance in later periods. Taken together, these findings show that changes in connectivity patterns were closely associated with changing ecological preferences and subsistence-related land-use strategies.

Across the full sequence considered here, the analyses do not support a single, uniform response of communication systems to environmental change. Instead, they show that connectivity, settlement concentration, and land-use organization varied across archaeological periods, climatic regimes, and ecological settings. The main interpretive lesson is therefore not that one environmental factor controlled connectivity, but that long-term communication systems in the Carpathian Basin must be understood through the combined influence of topography, hydrology, ecological setting, hydroclimatic variability, and subsistence practices.

The broader significance of the study lies in both its results and its approach. Empirically, it clarifies that diachronic connectivity in the Carpathian Basin was shaped by shifting relations between centers of high site intensity, peripheries, ecological opportunity spaces, and land-use strategies rather than by simple spatial continuity alone. Methodologically, the study's main novelty lies in integrating environmentally weighted network modelling, ecological classification, and bioarchaeological evidence within one comparative diachronic framework. This provides a robust basis for future work on mobility, settlement organization, human-environment interactions, and long-term socio-ecological adaptation, both in the Carpathian Basin and in other regions where dense archaeological and environmental records allow similarly integrated analyses.

Author contributions

MK: Conceptualization; Data curation; Formal analysis; Investigation; Methodology; Software; Visualization; Writing – original draft; Writing – review & editing.

JL: Writing – review & editing.

JP: Writing – review & editing.

UB: Writing – review & editing.

PB: Writing – review & editing.

AK: Data curation.

EX: Writing – review & editing.

MLCD: Data curation; Formal analysis; Investigation; Methodology; Software; Visualization; Writing – original draft; Writing – review & editing.

Code availability

All code to reproduce the analysis or customize the model is available from this repository after publication of the article. A fully reproducible dummy code with synthetic data to replicate the model can be accessed from this repository after publication of the article: Kempf, M., 2026b: Reproducible network and connectivity models. Zenodo. https://doi.org/10.5281/zenodo.20792095. Experimental code can be accessed from Kempf, M. (2026c). Data and code to Kempf, M. et al. (2026): Cross-chronological network models [Data set]. Zenodo. https://doi.org/10.5281/zenodo.17678714. The compiled dataset of published stable carbon and nitrogen isotope data of archaeological human and animal remains used for the isotope review as well as the related codes for the ANOVA tests and the Generalized Additive Models (GAM) are available in open access from: Depaermentier, M.L.C. (2026). Isotope dataset and R-codes to: KEMPF, M. et al. Adaptive connectivity networks across climatic and ecological regimes from the Neolithic to the Middle Ages in the Carpathian Basin (Version v1) [Data set]. Zenodo. https://doi.org/10.5281/zenodo.20810863.

Declaration of competing interest

The authors declare that they have no known competing financial interests or personal relationships that could have appeared to influence the work reported in this paper.

Acknowledgements

MK received a post-doctoral fellowship grant from the Swiss National Science Foundation (SNSF) at the University of Basel (CH) under the project number TMPFP2_217358, project *EXOCHAINS - Exploring Holocene Climate Change and Human Innovations across Eurasia*. MK and UB acknowledge support from the ERC Synergy project 101118880; Synergy-Plague. EX acknowledges support from the ERC Synergy project EUROpest under Grant Agreement number 101166700. JP acknowledges the project “Ready for the Future: Understanding the Long-Term Resilience of Human Culture” (CZ.02.01.01/00/22_008/0004593) and the Ministry of Education, Youth and Sports of the Czech Republic. MLCD acknowledges the support of the ERC CoG project 101087964 (MILWAYS), awarded to Giedre Motuzaite Matuzeviciute, Vilnius University.

Appendix A. Supplementary data

Supplementary data to this article can be found online at https://doi.org/10.1016/j.quascirev.2026.110152.

Data availability

A link to the data and/or code is provided as part of this submission. Isotope dataset and R-codes to: KEMPF, M. et al. Adaptive connectivity networks across climatic and ecological regimes from the Neolithic to the Middle Ages in the Carpathian Basin https://doi.org/10.5281/zenodo.20810863

References

Allentoft, M.E., Sikora, M., Sjögren, K.-G., Rasmussen, S., Rasmussen, M., Stenderup, J., Damgaard, P.B., Schroeder, H., Ahlström, T., Vinner, L., Malaspinas, A.-S., Margaryan, A., Higham, T., Chivall, D., Lynnerup, N., Harvig, L., Baron, J., Casa, P. D., Dąbrowski, P., Duffy, P.R., Ebel, A.V., Epimakhov, A., Frei, K., Furmanek, M., Gralak, T., Gromov, A., Gronkiewicz, S., Grupe, G., Hajdu, T., Jarysz, R., Khartanovich, V., Khokhlov, A., Kiss, V., Kolář, J., Kriiska, A., Lasak, I., Longhi, C., McGlynn, G., Merkevicius, A., Merkyte, I., Metspalu, M., Mkrtchyan, R., Moiseyev, V., Paja, L., Pálfi, G., Pokutta, D., Pospieszny, Ł., Price, T.D., Saag, L., Sablin, M., Shishlina, N., Smrčka, V., Soenov, V.I., Szeverényi, V., Tóth, G., Trifanova, S.V., Varul, L., Vicze, M., Yepiskoposyan, L., Zhitenev, V., Orlando, L., Sicheritz-Pontén, T., Brunak, S., Nielsen, R., Kristiansen, K., Willerslev, E., 2015. Population genomics of Bronze Age Eurasia. Nature 522, 167–172. https://doi.org/10.1038/nature14507.

Alley, R., Agustsdottir, A., 2005. The 8k event: cause and consequences of a major Holocene abrupt climate change. Quat. Sci. Rev. 24, 1123–1149. https://doi.org/10.1016/j.quascirev.2004.12.004.

Alt, K.W., Knipper, C., Peters, D., Müller, W., Maurer, A.-F., Kollig, I., Nicklisch, N., Müller, C., Karimnia, S., Brandt, G., Roth, C., Rosner, M., Mende, B., Schöne, B.R., Vida, T., Von Freeden, U., 2014. Lombards on the move – an integrative study of the migration period cemetery at Szólád, Hungary. PLoS One 9, e110793. https://doi.org/10.1371/journal.pone.0110793.

Amorim, C.E.G., Vai, S., Posth, C., Modi, A., Koncz, I., Hakenbeck, S., La Rocca, M.C., Mende, B., Bobo, D., Pohl, W., Baricco, L.P., Bedini, E., Francalacci, P., Giostra, C., Vida, T., Winger, D., Von Freeden, U., Ghirotto, S., Lari, M., Barbujani, G., Krause, J., Caramelli, D., Geary, P.J., Veeramah, K.R., 2018. Understanding 6th-century barbarian social organization and migration through paleogenomics. Nat. Commun. 9, 3547. https://doi.org/10.1038/s41467-018-06024-4.

Baddeley, A., Rubak, E., Turner, R., 2015. Spatial Point Patterns, Methodology and Applications with R. Chapman & Hall, New York. https://doi.org/10.1201/b19708.

Banffy, E., 2008. The boundary in western Transdanubia: variations of migration and adaptation. In: Living Well Together? Settlement and Materiality in the Neolithic of South-East and Central Europe. Oxbow, Oxford, pp. 151–163.

Banffy, E., 2013. The Early Neolithic in the Danube-Tisza Interfluve. Archaeopress, Oxford.

Banffy, E., Sümegi, P., 2012. The early Neolithic agro-ecological barrier in the carpathian Basin: a Zone for interaction. In: Archaeological, Cultural and Linguistic Heritage: Festschrift for Erzsébet Jerem in Honour of Her 70th Birthday. Archaeolingua, Budapest, pp. 57–69.

Bartosiewicz, L., 2003. A Millennium of migrations: Proto-historic Mobile pastoralism in Hungary. FLMNH 44, 101–130. https://doi.org/10.58782/flmnh.gtob8676.

Betti, L., Beyer, R.M., Jones, E.R., et al., 2020. Climate shaped how Neolithic farmers and European hunter-gatherers interacted after a major slowdown from 6,100 bce to 4,500 bce. Nat. Hum. Behav. 4, 1004–1010. https://doi.org/10.1038/s41562-020-0897-7.

Bilotti, G., Kempf, M., Morillo Leon, J.M., 2024. Modelling land and water based movement corridors in the Western Mediterranean: a least cost path analysis from chalcolithic and early bronze age ivory records. Archaeol. Anthropol. Sci. 16, 122. https://doi.org/10.1007/s12520-024-02029-x.

Bivand, R., 2023. Rgrass: interface between “GRASS” Geographical Information System and “R”. R package version 0 3–9.

Bánffy, E., 2015. The beginnings of salt exploitation in the Carpathian Basin (6th–5th millennium BC). Documenta Preahistorica 42. https://doi.org/10.4312/dp.42.13.

Bánffy, E., 2019. First farmers of the Carpathian Basin: changing patterns in subsistence, ritual and monumental figurines. Prehistoric Society Research Paper. Oxbow books The Prehistoric society, Oxford [London (GB)].

Büntgen, U., Myglan, V.S., Ljungqvist, F.C., McCormick, M., Di Cosmo, N., Sigl, M., Jungclaus, J., Wagner, S., Krusic, P.J., Esper, J., Kaplan, J.O., De Vaan, M.A.C., Luterbacher, J., Wacker, L., Tegel, W., Kirdyanov, A.V., 2016. Cooling and societal change during the Late Antique little ice age from 536 to around 660 AD. Nat. Geosci. 9, 231–236. https://doi.org/10.1038/ngeo2652.

Bodnariuc, A., Bouchette, A., Dedoubat, J.J., Otto, T., Fontugne, M., Jalut, G., 2002. Holocene vegetational history of the Apuseni mountains, central Romania. Quat. Sci. Rev. 21, 1465–1488. https://doi.org/10.1016/S0277-3791(01)00117-2.

Bonsall, C., Macklin, M.G., Boroneanţ, A., Pickard, C., Bartosiewicz, L., Cook, G.T., Higham, T.F.G., 2015. Holocene climate change and prehistoric settlement in the lower Danube valley. Quat. Int. 378, 14–21. https://doi.org/10.1016/j.quaint.2014.09.031.

Bradley, R.S., Hughes, M.K., Diaz, H.F., 2003. Climate in medieval time. Science 302, 404–405. https://doi.org/10.1126/science.1090372.

Brown, T., Bailey, G., Passmore, D., 2013. Environments and landscape change. In: The Oxford Handbook of Neolithic Europ. Oxford University Press, Oxford, pp. 27–60.

Brughmans, T., 2013. Thinking through networks: a review of formal network methods in archaeology. J. Archaeol. Method Theor 20, 623–662. https://doi.org/10.1007/s10816-012-9133-8.

Cavazzuti, C., Horváth, A., Gémes, A., Fülöp, K., Szeniczey, T., Tarbay, J.G., McCall, A., Rubio, B.G., Vicze, M., Bárány, A., Pető, Á., Magyari, E.K., Darabos, G., Futó, I., Lisztes-Szabó, Z., Molnár, E., Novak, M., Gál, E., Fischl, K.P., Kulcsár, G., Szeverényi, V., Szabó, G., Mester, E., Dani, J., Palcsu, L., Kiss, V., Major, I., Hajdu, T., 2025. Isotope and archaeobotanical analysis reveal radical changes in mobility, diet and inequalities around 1500 BCE at the core of Europe. Sci. Rep. 15, 17494. https://doi.org/10.1038/s41598-025-01113-z.

Chapman, J., Magyari, E., Gaydarska, B., 2009. Contrasting subsistence strategies in the early Iron Age? - new results from the Alfold Plain, Hungary, and the Thracian Plain, Bulgaria. Oxf. J. Archaeol. 28, 155–187. https://doi.org/10.1111/j.1468-0092.2009.00323.x.

Clarke, E., Sherrill-Mix, S., Dawson, C., 2025. Ggbeeswarm: Categorical Scatter (Violin Point) Plots. https://doi.org/10.32614/CRAN.package.ggbeeswarm, 0.7.3.

Cocozza, C., Cirelli, E., Groß, M., Teegen, W.-R., Fernandes, R., 2022. Presenting the compendium isotoporum Medii aevi, a multi-isotope database for medieval Europe. Sci. Data 9, 354. https://doi.org/10.1038/s41597-022-01462-8.

Collar, A., Coward, F., Brughmans, T., et al., 2015. Networks in archaeology: Phenomena, abstraction, representation. J. Archaeol. Method Theor 22, 1–32. https://doi.org/10.1007/s10816-014-9235-6.

Conolly, J., Lake, M., 2006. Geographical Information Systems in Archaeology, first ed. Cambridge University Press. https://doi.org/10.1017/CBO9780511807459.

Depaermentier, M.L.C., 2026. Isotope dataset and R-codes to: KEMPF, M. et al. Adaptive connectivity networks across climatic and ecological regimes from the Neolithic to the Middle Ages in the Carpathian Basin (Version v1). Zenodo [Data set]. https://doi.org/10.5281/zenodo.20810863.

Depaermentier, M.L.C., Makarowicz, P., Szczepanek, A., Snoeck, C., Morvan, M., Belka, Z., Kempf, M., Pospieszny, Ł., Taras, H., Chyleński, M., Górski, J., Goslar, T., Grygiel, R., Jarosz, P., Juras, A., Lasota-Kuś, A., Matoga, A., Nowak, M., Przybyła, M.M., Tunia, K., Włodarczak, P., Wilczyński, J., Wójcik, I., Motuzaitė Matuzevičiūtė, G., In preparation. Multi-proxy bioarchaeological analyses reveal subsistence shift in Bronze Age Central Europe. Sci. Adv. (under review).

Depaermentier, M.L.C., Kempf, M., Bánffy, E., Alt, K.W., 2021. Modelling a scale-based strontium isotope baseline for Hungary. J. Archaeol. Sci. 135, 105489. https://doi.org/10.1016/j.jas.2021.105489.

Depaermentier, M.L.C., Kempf, M., Bánffy, E., Alt, K.W., 2025a. Cultural diversity shaped neolithic subsistence in the Carpathian Basin. Sci. Rep. 15, 4281. https://doi.org/10.1038/s41598-025-88541-z.

Depaermentier, M.L.C., Kempf, M., Motuzaite Matuzeviciute, G., 2025b. Environmentally adjusted δ13C thresholds for accurate detection of C4 plant consumption in Europe. Commun. Earth Environ. 6, 1021. https://doi.org/10.1038/s43247-025-03031-4.

Depaermentier, M.L.C., Kempf, M., Vander Linden, M., Britton, K., Madgwick, R., Büntgen, U., Drucker, D.G., Jones, J.R., Snoeck, C., Stevens, R.E., 2025c. The palaeoenvironmental potential of bioarchaeological isotope data. Commun. Earth Environ. 6, 501. https://doi.org/10.1038/s43247-025-02507-7.

Depaermentier, M.L.C., Osztás, A., Bánffy, E., Alt, K.W., Kempf, M., 2020b. Neolithic land-use, subsistence, and mobility patterns in Transdanubia: a multiproxy isotope and environmental analysis from Alsónyék – Bátaszék and Mórágy – tűzkődomb. J. Archaeolog. Sci.: Rep. 33, 102529. https://doi.org/10.1016/j.jasrep.2020.102529.

Depaermentier, Margaux L.C., Kempf, M., Bánffy, E., Alt, K.W., 2020a. Tracing mobility patterns through the 6th-5th millennia BC in the Carpathian Basin with strontium and oxygen stable isotope analyses. PLoS One 15, e0242745. https://doi.org/10.1371/journal.pone.0242745.

Dermody, B.J., Van Beek, R.P.H., Meeks, E., Klein Goldewijk, K., Scheidel, W., Van Der Velde, Y., Bierkens, M.F.P., Wassen, M.J., Dekker, S.C., 2014. A virtual water network of the Roman world. Hydrol. Earth Syst. Sci. 18, 5025–5040. https://doi.org/10.5194/hess-18-5025-2014.

Dreslerová, D., Kočár, P., Chuman, T., Pokorná, A., 2017. Cultivation with deliberation: cereals and their growing conditions in prehistory. Veg. Hist. Archaeobotany 26, 513–526. https://doi.org/10.1007/s00334-017-0609-z.

Dreslerová, D., Kočár, P., Chuman, T., Šefrna, L., Poništiak, Š., 2013. Variety in cereal cultivation in the Late bronze and early iron Ages in relation to environmental conditions. J. Archaeol. Sci. 40, 1988–2000. https://doi.org/10.1016/j.jas.2012.12.010.

Ducke, B., Suchowska, P., 2022. Exploratory network reconstruction with sparse archaeological data and XTENT. J. Archaeol. Method Theor 29, 508–539. https://doi.org/10.1007/s10816-021-09529-3.

Duffy, P.R., 2020. River networks and funerary metal in the Bronze Age of the Carpathian basin. PLoS One 15, e0238526. https://doi.org/10.1371/journal.pone.0238526.

Essell, H., Krusic, P.J., Esper, J., Wagner, S., Braconnot, P., Jungclaus, J., Muschitiello, F., Oppenheimer, C., Büntgen, U., 2023. A frequency-optimised temperature record for the Holocene. Environ. Res. Lett. 18, 114022. https://doi.org/10.1088/1748-9326/ad0065.

European Environment Agency, 2019. EU-Hydro River Network Database 2006-2012 (Vector). https://doi.org/10.2909/393359A7-7EBD-4A52-80AC-1A18D5F3DB9C. Europe - version 1.3, Nov. 2020.

Fernández-Götz, M., 2018. Urbanization in Iron Age Europe: trajectories, patterns, and social dynamics. J. Archaeol. Res. 26, 117–162. https://doi.org/10.1007/s10814-017-9107-1.

Feurdean, A., Klotz, S., Mosbrugger, V., Wohlfarth, B., 2008. Pollen-based quantitative reconstructions of Holocene climate variability in NW Romania. Palaeogeogr. Palaeoclimatol. Palaeoecol. 260, 494–504. https://doi.org/10.1016/j.palaeo.2007.12.014.

Feurdean, A., Liakka, J., Vannière, B., Marinova, E., Hutchinson, S.M., Mosburgger, V., Hickler, T., 2013. 12,000-Years of fire regime drivers in the lowlands of Transylvania (Central-Eastern Europe): a data-model approach. Quat. Sci. Rev. 81, 48–61. https://doi.org/10.1016/j.quascirev.2013.09.014.

Fick, S.E., Hijmans, R.J., 2017. WorldClim 2: new 1-km spatial resolution climate surfaces for global land areas. Int J Climatolo 37, 4302–4315. https://doi.org/10.1002/joc.5086.

Filipović, D., Meadows, J., Corso, M.D., Kirleis, W., Alsleben, A., Akeret, Ö., Bittmann, F., Bosi, G., Ciută, B., Dreslerová, D., Effenberger, H., Gyulai, F., Heiss, A.G., Hellmund, M., Jahns, S., Jakobitsch, T., Kapcia, M., Klooß, S., Kohler-Schneider, M., Kroll, H., Makarowicz, P., Marinova, E., Märkle, T., Medović, A., Mercuri, A.M., Mueller-Bieniek, A., Nisbet, R., Pashkevich, G., Perego, R., Pokorný, P., Pospieszny, Ł., Przybyła, M., Reed, K., Rennwanz, J., Stika, H.-P., Stobbe, A., Tolar, T., Wasylikowa, K., Wiethold, J., Zerl, T., 2020. New AMS 14C dates track the arrival and spread of broomcorn millet cultivation and agricultural change in prehistoric Europe. Sci. Rep. 10, 13698. https://doi.org/10.1038/s41598-020-70495-z.

Fort, J., 2022. Dispersal distances and cultural effects in the spread of the Neolithic along the northern mediterranean coast. Archaeol. Anthropol. Sci. 14, 153. https://doi.org/10.1007/s12520-022-01619-x.

Gastwirth, J.L., 1972. The estimation of the Lorenz curve and gini index. Rev. Econ. Stat. 54, 306. https://doi.org/10.2307/1937992.

Gaudenyi, T., Mihajlović, M., 2022. The carpathian basin: denomination and delineation. EJGEO 3, 1–6. https://doi.org/10.24018/ejgeo.2022.3.2.239.

Gelabert, P., Bickle, P., Hofmann, D., Teschler-Nicola, M., Anders, A., Huang, X., Hämmerle, M., Olalde, I., Fournier, R., Ringbauer, H., Akbari, A., Cheronet, O., Lazaridis, I., Broomandkhoshbacht, N., Fernandes, D.M., Buttinger, K., Callan, K., Candilio, F., Bravo Morante, G., Curtis, E., Ferry, M., Keating, D., Freilich, S., Kearns, A., Harney, É., Lawson, A.M., Mandl, K., Michel, M., Oberreiter, V., Zagorc, B., Oppenheimer, J., Sawyer, S., Schattke, C., Özdoğan, K.T., Qiu, L., Workman, J.N., Zalzala, F., Mallick, S., Mah, M., Micco, A., Pieler, F., Pavuk, J., Šefčáková, A., Lazar, C., Starović, A., Djuric, M., Krznarić Škrivanko, M., Šlaus, M., Bedić, Ž., Novotny, F., D. Szabó, L., Cserpák-Laczi, O., Hága, T., Szolnoki, L., Hajdú, Z., Mirea, P., Nagy, E.G., Virág, Z.M., Horváth, M.A., Horváth, L.A., T. Biró, K., Domboróczki, L., Szeniczey, T., Jakucs, J., Szelekovszky, M., Zoltán, F., Sztáncsuj, S.J., Tóth, K., Csengeri, P., Pap, I., Patay, R., Putica, A., Vasov, B., Havasi, B., Sebők, K., Raczky, P., Lovász, G., Tvrdý, Z., Rohland, N., Novak, M., Ruttkay, M., Krošláková, M., Bátora, J., Paluch, T., Borić, D., Dani, J., Kuhlwilm, M., Palamara, P.F., Hajdu, T., Pinhasi, R., Reich, D., 2024. Social and genetic diversity in first farmers of central Europe. Nat. Hum. Behav. 9, 53–64. https://doi.org/10.1038/s41562-024-02034-z.

Goosse, H., Arzel, O., Luterbacher, J., Mann, M.E., Renssen, H., Riedwyl, N., Timmermann, A., Xoplaki, E., Wanner, H., 2006. The origin of the European "Medieval Warm Period.". Clim. Past 2, 99–113. https://doi.org/10.5194/cp-2-99-2006.

Graham, N.E., Ammann, C.M., Fleitmann, D., Cobb, K.M., Luterbacher, J., 2011. Support for global climate reorganization during the "Medieval Climate Anomaly.". Clim. Dyn. 37, 1217–1245. https://doi.org/10.1007/s00382-010-0914-z.

Gronenborn, D., Strien, H.-C., Dietrich, S., Sirocko, F., 2014. 'Adaptive Cycles' and climate fluctuations: a case study from Linear pottery culture in Western central Europe. J. Archaeol. Sci. 51, 73–83. https://doi.org/10.1016/j.jas.2013.03.015.

Gugora, A., Dupras, T.L., Fóthi, E., Demény, A., 2021. New home, new diet? Reconstruction of diet at the 10th century CE Hungarian Conquest period site of Kenézlő-Fazekaszug from stable carbon and nitrogen isotope analyses. J. Archaeolog. Sci.: Rep. 38, 103033. https://doi.org/10.1016/j.jasrep.2021.103033.

Gyucha, A., Riebe, D.J., Viktorik, O., Máté, L., Kreiter, A., 2024. Potters' technological choices in turbulent times: exploring the transition from the Neolithic to the Copper Age on the great Hungarian Plain through communities of practice and technological investment theories. J. Anthropol. Archaeol. 76, 101622. https://doi.org/10.1016/j.jaa.2024.101622.

Haak, W., Lazaridis, I., Patterson, N., Rohland, N., Mallick, S., Llamas, B., Brandt, G., Nordenfelt, S., Harney, E., Stewardson, K., Fu, Q., Mittnik, A., Bánffy, E., Economou, C., Francken, M., Friederich, S., Pena, R.G., Hallgren, F., Khartanovich, V., Khokhlov, A., Kunst, M., Kuznetsov, P., Meller, H., Mochalov, O., Moiseyev, V., Nicklisch, N., Pichler, S.L., Risch, R., Rojo Guerra, M.A., Roth, C., Szécsényi-Nagy, A., Wahl, J., Meyer, M., Krause, J., Brown, D., Anthony, D., Cooper, A., Alt, K.W., Reich, D., 2015. Massive migration from the steppe was a source for Indo-European languages in Europe. Nature 522, 207–211. https://doi.org/10.1038/nature14317.

Hakenbeck, S.E., Evans, J., Chapman, H., Fóthi, E., 2017. Practising pastoralism in an agricultural environment: an isotopic analysis of the impact of the Hunnic incursions on Pannonian populations. PLoS One 12, e0173079. https://doi.org/10.1371/journal.pone.0173079.

Halsall, G., 2014. Two worlds become one: a "Counter-Intuitive" View of the Roman Empire and "Germanic" migration. Ger. Hist. 32, 515–532. https://doi.org/10.1093/gerhis/ghu107.

Helama, S., Jones, P.D., Briffa, K.R., 2017. Limited late Antique cooling. Nat. Geosci. 10, 242–243. https://doi.org/10.1038/ngeo2926.

Herzog, I., 2014. A review of case studies in archaeological least-cost analysis. Archeologia e Calcolatori 25, 223–239. https://doi.org/10.19282/ac.25.2014.12.

Hou, M., Wu, W., Cohen, D.J., Zeng, Z., Huang, H., Zheng, H., Ge, Q., 2023. Detection of a mid-holocene climate event at 7.2 ka BP based on an analysis of globally-distributed multi-proxy records. Palaeogeogr. Palaeoclimatol. Palaeoecol. 618, 111525. https://doi.org/10.1016/j.palaeo.2023.111525.

Ionita, M., 2014. The impact of the East Atlantic/Western Russia pattern on the hydroclimatology of Europe from mid-winter to late spring. Climate 2, 296–309. https://doi.org/10.3390/cli2040296.

Jakucs, J., Bánffy, E., Oross, K., Voicsek, V., Bronk Ramsey, C., Dunbar, E., Kromer, B., Bayliss, A., Hofmann, D., Marshall, P., Whittle, A., 2016. Between the vinča and

Linearbandkeramik Worlds: the diversity of practices and identities in the 54th–53rd centuries cal BC in Southwest Hungary and beyond. J World Prehist 29, 267–336. https://doi.org/10.1007/s10963-016-9096-x.
Kemenczei, T., 2003. The Iron Age. The beginning of the Iron Age: the pre-scythians (8th century B.C.). In: Hungarian Archaeology at the Turn of the Millennium. Ministry of National Cultural Heritage Teleki László Foundation, Budapest, pp. 177–179.
Kempf, M., 2020. Neolithic land-use, landscape development, and environmental dynamics in the Carpathian Basin. J. Archaeolog. Sci.: Rep. 34, 102637. https://doi.org/10.1016/j.jasrep.2020.102637.
Kempf, M., 2021. Take a seed! Revealing Neolithic landscape and agricultural development in the Carpathian Basin through multivariate statistics and environmental modelling. PLoS One 16, e0258206. https://doi.org/10.1371/journal.pone.0258206.
Kempf, M., Depaermentier, M.L.C., Spengler Iii, R.N., Frachetti, M.D., Chen, F., Luterbacher, J., Xoplaki, E., Büntgen, U., 2025. Hydroclimatic instability accelerated the socio-political decline of the Tang Dynasty in northern China. Commun. Earth Environ. 6, 1003. https://doi.org/10.1038/s43247-025-03038-x.
Kempf, M., 2026a. Global to regional ecozone classifications from multivariate clustering models. Ecol. Inform. 96, 103840. https://doi.org/10.1016/j.ecoinf.2026.103840.
Kempf, M., Denis, S., 2024. Resource dependency and communication networks in early Neolithic western Europe. Quat Environ Humans 2, 100014. https://doi.org/10.1016/j.qeh.2024.100014.
Kempf, M., Günther, G., 2023. Point pattern and spatial analyses using archaeological and environmental data – a case study from the Neolithic Carpathian Basin. J. Archaeolog. Sci.: Rep. 47, 103747. https://doi.org/10.1016/j.jasrep.2022.103747.
Kempf, M., 2026b. Reproducible network and connectivity models. Zenodo. https://doi.org/10.5281/zenodo.20792095.
Kempf, M., 2026c. Data and code to Kempf, M. et al. (2026): Cross-chronological network models. Zenodo [Data set]. https://doi.org/10.5281/zenodo.17678714.
Kiss, T., Sümeghy, B., Sipos, G., 2014. Late Quaternary paleodrainage reconstruction of the Maros River alluvial fan. Geomorphology 204, 49–60. https://doi.org/10.1016/j.geomorph.2013.07.028.
Knipl, I., Sümegi, P., 2012. Life at the interface of two distinct landscapes-relationship of humans and environment in the periphery of the Danube-Tisza Interfluve between Hajós and Császártöltés. Open Geosci. 4, 439–447. https://doi.org/10.2478/s13533-011-0071-x.
Knipper, C., Koncz, I., Ódor, J.G., Mende, B.G., Rácz, Z., Kraus, S., Van Gyseghem, R., Friedrich, R., Vida, T., 2020. Coalescing traditions—Coalescing people: community formation in Pannonia after the decline of the Roman Empire. PLoS One 15, e0231760. https://doi.org/10.1371/journal.pone.0231760.
Kreiter, A., 2021. The Hungarian archaeology database. Internet Archaeol. https://doi.org/10.11141/ia.58.9.
Kulcsár, G., Szeverényi, V., 2013. Transition to the Bronze Age: issues of continuity and discontinuity in the first half of the third millennium BC in the carpathian Basin. In: Transitions to the Bronze Age. Interregional Interaction and Socio-Cultural Change in the Third Millennium BC Carpathian Basin and Neighbouring Regions. Archaeolingua, Budapest.
Lazaridis, I., Patterson, N., Anthony, D., Vyazov, L., Fournier, R., Ringbauer, H., Olalde, I., Khokhlov, A.A., Kitov, E.P., Shishlina, N.I., Ailincăi, S.C., Agapov, D.S., Agapov, S.A., Batieva, E., Bauyrzhan, B., Bereczki, Z., Buzhilova, A., Changmai, P., Chizhevsky, A.A., Ciobanu, I., Constantinescu, M., Csányi, M., Dani, J., Dashkovskiy, P.K., Évinger, S., Faifert, A., Flegontov, P., Frînculeasa, A., Frînculeasa, M.N., Hajdu, T., Higham, T., Jarosz, P., Jelínek, P., Khartanovich, V.I., Kirginekov, E.N., Kiss, V., Kitova, A., Kiyashko, A.V., Koledin, J., Korolev, A., Kosintsev, P., Kulcsár, G., Kuznetsov, P., Magomedov, R., Mamedov, A.M., Melis, E., Moiseyev, V., Molnár, E., Monge, J., Negrea, O., Nikolaeva, N.A., Novak, M., Ochir-Goryaeva, M., Pálfi, G., Popovici, S., Rykun, M.P., Savenkova, T.M., Semibratov, V. P., Seregin, N.N., Šefčáková, A., Mussayeva, R.S., Shingiray, I., Shirokov, V.N., Simalcsik, A., Sirak, K., Solodovnikov, K.N., Tárnoki, J., Tishkin, A.A., Trifonov, V., Vasilyev, S., Akbari, A., Brielle, E.S., Callan, K., Candilio, F., Cheronet, O., Curtis, E., Flegontova, O., Iliev, L., Kearns, A., Keating, D., Lawson, A.M., Mah, M., Micco, A., Michel, M., Oppenheimer, J., Qiu, L., Workman, J.N., Zalzala, F., Szécsényi-Nagy, A., Palamara, P.F., Mallick, S., Rohland, N., Pinhasi, R., Reich, D., 2025. The genetic origin of the Indo-Europeans. Nature 639, 132–142. https://doi.org/10.1038/s41586-024-08531-5.
Lee-Thorp, J.A., 2008. On isotopes and old bones. Archaeometry 50, 925–950. https://doi.org/10.1111/j.1475-4754.2008.00441.x.
Lehmkuhl, F., Nett, J.J., Pötter, S., et al., 2021. Loess landscapes of Europe – mapping, geomorphology, and zonal differentiation. Earth Sci. Rev. https://doi.org/10.1016/j.earscirev.2020.103496.
Leonardi, M., Hallett, E.Y., Beyer, R.M., Krapp, M., Manica, A., 2023. Pastclim 1.2: an R package to easily access and use paleoclimatic reconstructions. Ecography, e06481. https://doi.org/10.1111/ecog.06481, 2023.
Levanič, T., Popa, I., Poljanšek, S., Nechita, C., 2013. A 323-year long reconstruction of drought for SW Romania based on black pine (Pinus Nigra) tree-ring widths. Int. J. Biometeorol. 57, 703–714. https://doi.org/10.1007/s00484-012-0596-9.
Lipson, M., Szécsényi-Nagy, A., Mallick, S., Pósa, A., Stégmár, B., Keerl, V., Rohland, N., Stewardson, K., Ferry, M., Michel, M., Oppenheimer, J., Broomandkhoshbacht, N., Harney, E., Nordenfelt, S., Llamas, B., Gusztáv Mende, B., Köhler, K., Oross, K., Bondár, M., Marton, T., Osztás, A., Jakucs, J., Paluch, T., Horváth, F., Csengeri, P., Koós, J., Sebők, K., Anders, A., Raczky, P., Regenye, J., Barna, J.P., Fábián, S., Serlegi, G., Toldi, Z., Gyöngyvér Nagy, E., Dani, J., Molnár, E., Pálfi, G., Márk, L., Melegh, B., Bánfai, Z., Domboróczki, L., Fernández-Eraso, J., Antonio Mujika-Alustiza, J., Alonso Fernández, C., Jiménez Echevarría, J., Bollongino, R., Orschiedt, J., Schierhold, K., Meller, H., Cooper, A., Burger, J., Bánffy, E., Alt, K.W., Lalueza-Fox, C., Haak, W., Reich, D., 2017. Parallel palaeogenomic transects reveal complex genetic history of early European farmers. Nature 551, 368–372. https://doi.org/10.1038/nature24476.
Lovelace, R., Ellison, R., 2019. Stplanr: a package for transport planning. R J. 10, 7. https://doi.org/10.32614/RJ-2018-053.
Luterbacher, J., Werner, J.P., Smerdon, J.E., Fernández-Donado, L., González-Rouco, F. J., Barriopedro, D., Ljungqvist, F.C., Büntgen, U., Zorita, E., Wagner, S., Esper, J., McCarroll, D., Toreti, A., Frank, D., Jungclaus, J.H., Barriendos, M., Bertolin, C., Bothe, O., Brázdil, R., Camuffo, D., Dobrovolný, P., Gagen, M., García-Bustamante, E., Ge, Q., Gómez-Navarro, J.J., Guiot, J., Hao, Z., Hegerl, G.C., Holmgren, K., Klimenko, V.V., Martín-Chivelet, J., Pfister, C., Roberts, N., Schindler, A., Schurer, A., Solomina, O., Von Gunten, L., Wahl, E., Wanner, H., Wetter, O., Xoplaki, E., Yuan, N., Zanchettin, D., Zhang, H., Zerefos, C., 2016. European summer temperatures since Roman times. Environ. Res. Lett. 11, 024001. https://doi.org/10.1088/1748-9326/11/2/024001.
Magyari, E.K., Raczky, P., Merkl, M., Pálfi, I., Darabos, G., Hajnalova, M., Moskal-Hoyo, M., 2024. Review on vegetation, landscape and climate changes in the Carpathian Basin during the Neolithic and chalcolithic period. Veg. Hist. Archaeobotany 33, 769–794. https://doi.org/10.1007/s00334-024-00986-w.
Maróti, Z., Neparáczki, E., Schütz, O., Maár, K., Varga, G.I.B., Kovács, B., Kalmár, T., Nyerki, E., Nagy, I., Latinovics, D., Tihanyi, B., Marcsik, A., Pálfi, G., Bernert, Z., Gallina, Z., Horváth, C., Varga, S., Költő, L., Raskó, I., Nagy, P.L., Balogh, C., Zink, A., Maixner, F., Götherström, A., George, R., Szalontai, C., Szenthe, G., Gáll, E., Kiss, A.P., Gulyás, B., Kovacsóczy, B.Ny, Gál, S.S., Tomka, P., Török, T., 2022. The genetic origin of Huns, Avars, and conquering Hungarians. Curr. Biol. 32, 2858–2870.e7. https://doi.org/10.1016/j.cub.2022.04.093.
McCall, A., Gamarra, B., Carlson, K.S.D., Bernert, Z., Cséki, A., Csengeri, P., Domboróczki, L., Endrődi, A., Hellebrandt, M., Horváth, A., Király, Á., Kiss, K., Koós, J., Kovács, P., Köhler, K., Szolnoki, L., Zoffmann, Z.K., Sirak, K., Szeniczey, T., Dani, J., Hajdu, T., Pinhasi, R., 2022. Stable carbon and nitrogen isotopes identify nuanced dietary changes from the Bronze and Iron ages on the great Hungarian Plain. Sci. Rep. 12, 16982. https://doi.org/10.1038/s41598-022-21138-y.
McKay, N.P., Kaufman, D.S., Arcusa, S.H., Kolus, H.R., Edge, D.C., Erb, M.P., Hancock, C. L., Routson, C.C., Żarczyński, M., Marshall, L.P., Roberts, G.K., Telles, F., 2024. The 4.2 ka event is not remarkable in the context of Holocene climate variability. Nat. Commun. 15, 6555. https://doi.org/10.1038/s41467-024-50886-w.
Miller, N.F., Spengler, R.N., Frachetti, M., 2016. Millet cultivation across Eurasia: origins, spread, and the influence of seasonal climate. Holocene 26, 1566–1575. https://doi.org/10.1177/0959683616641742.
Morrill, C., LeGrande, A.N., Renssen, H., Bakker, P., Otto-Bliesner, B.L., 2013. Model sensitivity to North Atlantic freshwater forcing at 8.2 ka. Clim. Past 9, 955–968. https://doi.org/10.5194/cp-9-955-2013.
Nagavciuc, V., Scholz, P., Ionita, M., 2022. Hotspots for warm and dry summers in Romania. Nat. Hazards Earth Syst. Sci. 22, 1347–1369. https://doi.org/10.5194/nhess-22-1347-2022.
Nan, Q., Chen, S., Huang, L., Chen, L., Luterbacher, J., Meadows, M.E., 2026. Reassessing the global statistical significance of the 4.2 ka and 8.2 ka events from a spatial heterogeneity perspective. Sci. Bull.
Nan, Q., Chen, S., Liu, X., Ma, S., Sun, Y., Huang, L., Chen, J., Luterbacher, J., Meadows, M.E., Chen, F., 2025. The 4.2 ka event in the Northern Hemisphere: spatial heterogeneity and driving mechanisms of hydroclimatic change. Earth Sci. Rev. 265, 105128. https://doi.org/10.1016/j.earscirev.2025.105128.
O'Shea, J.M., 2011. A River runs through it: landscape and the evolution of Bronze Age networks in the carpathian Basin. J World Prehist 24, 161–174. https://doi.org/10.1007/s10963-011-9046-6.
OpenTopography, 2013. Shuttle Radar Topography mission (SRTM) global. https://doi.org/10.5069/G9445JDF.
Orfanou, E., Ghalichi, A., Rohrlach, A.B., Paust, E., Andrades Valtueña, A., Ernée, M., Furmanek, M., Hałuszko, A., Hermes, T., Himmel, M., Ilgner, J., Krause, J., Küßner, M., Lamnidis, T.C., Lucas, M., Adámková Malyková, D., Meller, H., Neumann, G.U., Papac, L., Penske, S., Salinger, M., Schrader, S.A., Schunke, T., Semerau, L., Smejtek, L., Traverso, L., Zach, B., Spengler, R., Stockhammer, P.W., Wahl, J., Snoeck, C., Ettel, P., Schneider, F.N., Roberts, P., Haak, W., 2026. Reconstruction of the lifeways of central european late Bronze Age communities using ancient DNA, isotope and osteoarchaeological analyses. Nat. Commun. 17, 1992. https://doi.org/10.1038/s41467-026-69895-y.
Oross, K., Jakucs, J., Marton, T., Gal, E., Whittle, A., 2023. Pioneers, carpenters, outsiders: radiocarbon dating of early farmers in western Hungary, in: relatively absolute. Relative and Absolute Chronologies in the Neolithic of Southeast Europe. Institute for Balkan Studies Serbian Academy of Sciences and Arts Special Edition, Belgrade, pp. 135–258.
Oross, K., Bánffy, E., 2009. Three successive waves of neolithisation: LBK development in Transdanubia. Doc. praeh. 36, 175–189. https://doi.org/10.4312/dp.36.11.
Panait, A., Diaconu, A., Galka, M., Grindean, R., Hutchinson, S., Hickler, T., Lamentowicz, M., Mulch, A., Tanţău, I., Werner, C., Feurdean, A., 2017. Hydrological conditions and carbon accumulation rates reconstructed from a mountain raised bog in the Carpathians: a multi-proxy approach. Catena 152, 57–68. https://doi.org/10.1016/j.catena.2016.12.023.
Parker, S.E., Harrison, S.P., 2022. The timing, duration and magnitude of the 8.2 ka event in global speleothem records. Sci. Rep. 12, 10542. https://doi.org/10.1038/s41598-022-14684-y.
Pawley, S., 2023. Rsagacmd: linking R with the open-source "SAGA-GIS" software_. R package version 0.4.2.
Perşoiu, A., Ionita, M., Weiss, H., 2019. Atmospheric blocking induced by the strengthened Siberian High led to drying in west Asia during the 4.2 ka BP event – a hypothesis. Clim. Past 15, 781–793. https://doi.org/10.5194/cp-15-781-2019.

Perşoiu, A., Onac, B.P., Wynn, J.G., Blaauw, M., Ionita, M., Hansson, M., 2017. Holocene winter climate variability in Central and Eastern Europe. Sci. Rep. 7, 1196. https://doi.org/10.1038/s41598-017-01397-w.

Petřík, J., Petr, L., Hanáček, M., Adameková, K., Kele, S., Milovský, R., Tóth, P., Bátora, J., Kučera, L., Světlík, I., Hutňan Chattová, B., Nohálová, H., Dubjelová, N., Majorošová, K., Xoplaki, E., Luterbacher, J., Synková, H., Nota, K., Kempf, M., 2026. Climatic Instability Coincided with the Mesolithic–Neolithic Transition in Central Europe. preparation.

Petrie, C.A., Jürcke, F.K., Wilkinson, T.C., et al., 2026. Over the hills and far away: modeling mobility and connectivity across the Iranian Plateau in late prehistory (c. 10,000–2000 BC) using multi-factor probabilistic corridors. J. Archaeol. Res. https://doi.org/10.1007/s10814-026-09221-8.

Pokorný, P., Chytrý, M., Juřičková, L., Sádlo, J., Novák, J., Ložek, V., 2015. Mid-Holocene bottleneck for central European dry grasslands: did steppe survive the forest optimum in northern Bohemia, Czech Republic? Holocene 25, 716–726. https://doi.org/10.1177/0959683614566218.

Popa, I., Kern, Z., 2009. Long-term summer temperature reconstruction inferred from tree-ring records from the Eastern Carpathians. Clim. Dyn. 32, 1107–1117. https://doi.org/10.1007/s00382-008-0439-x.

Pásztor, L., Laborczi, A., Bakacsi, Z., Szabó, J., Illés, G., 2018. Compilation of a national soil-type map for Hungary by sequential classification methods. Geoderma 311, 93–108. https://doi.org/10.1016/j.geoderma.2017.04.018.

Roibu, C.-C., Nagavciuc, V., Ionita, M., Popa, I., Horodnic, S.-A., Mursa, A., Büntgen, U., 2022. A tree ring-based hydroclimate reconstruction for eastern Europe reveals large-scale teleconnection patterns. Clim. Dyn. 59, 2979–2994. https://doi.org/10.1007/s00382-022-06255-8.

Salesse, K., Fernandes, R., De Rochefort, X., Brůžek, J., Castex, D., Dufour, É., 2018. IsoArcH.eu: an open-access and collaborative isotope database for bioarchaeological samples from the Graeco-Roman world and its margins. J. Archaeolog. Sci.: Rep. 19, 1050–1055. https://doi.org/10.1016/j.jasrep.2017.07.030.

Scheidel, W., 2015. Orbis: the Stanford geospatial network model of the roman world. SSRN Journal. https://doi.org/10.2139/ssrn.2609654.

Seppä, H., Birks, H.J.B., Giesecke, T., Hammarlund, D., Alenius, T., Antonsson, K., Bjune, A.E., Heikkilä, M., MacDonald, G.M., Ojala, A.E.K., Telford, R.J., Veski, S., 2007. Spatial structure of the 8200 cal yr BP event in northern Europe. Clim. Past 3, 225–236. https://doi.org/10.5194/cp-3-225-2007.

Seppä, H., Bjune, A.E., Telford, R.J., Birks, H.J.B., Veski, S., 2009. Last nine-thousand years of temperature variability in Northern Europe. Clim. Past 5, 523–535. https://doi.org/10.5194/cp-5-523-2009.

Strouhalová, B., Gebhardt, A., Ertlen, D., Šefrna, L., Flašarová, K., Kolařík, P., Schwartz, D., 2020. From Chernozem to Luvisol or from Luvisol to Chernozem? A discussion about the relationships and limits of the two types of soils. A case study of the soil catena of Hrušov, Czechia. Geografie 125, 473–500. https://doi.org/10.37040/geografie2020125040473.

Tobler, W., 1993. Three presentations on geographical analysis and modeling: Non-isotropic geographic modeling; speculations on the geometry of geography; and global spatial analysis (No. 93_1). NCGIA Tech. Rep.

Tóth, T., 2010. Salt-Affected soils and their native vegetation in Hungary. In: Öztürk, M., Böer, B., Barth, H.J., Clüsener-Godt, M., Khan, M., Breckle, S.W. (Eds.), Sabkha Ecosystems. Tasks for Vegetation Science, vol. 46. Springer, Dordrecht. https://doi.org/10.1007/978-90-481-9673-9_13.

Van Dijk, E., Jungclaus, J., Lorenz, S., Timmreck, C., Krüger, K., 2022. Was there a volcanic-induced long-lasting cooling over the Northern Hemisphere in the mid-6th–7th century? Clim. Past 18, 1601–1623. https://doi.org/10.5194/cp-18-1601-2022.

van Klinken, G.J., Richards, M.P., Hedges, R.E.M., 2002. An overview of causes for stable isotopic variations in past European human populations. Environmental, ecophysiological, and cultural effects. In: Ambrose, S.H., Katzenberg, M.A. (Eds.), Biogeochemical Approaches to Paleodietary Analysis, vol. 5. AAMS, New York and London, pp. 39–63.

Verhagen, P., Nuninger, L., Groenhuijzen, M.R., 2019. Modelling of pathways and movement networks in archaeology: an overview of Current approaches. In: Verhagen, P., Joyce, J., Groenhuijzen, M.R. (Eds.), Finding the Limits of the *Limes*. Computational Social Sciences. Springer, Cham. https://doi.org/10.1007/978-3-030-04576-0_11.

Wanner, H., Beer, J., Bütikofer, J., Crowley, T.J., Cubasch, U., Flückiger, J., Goosse, H., Grosjean, M., Joos, F., Kaplan, J.O., Küttel, M., Müller, S.A., Prentice, I.C., Solomina, O., Stocker, T.F., Tarasov, P., Wagner, M., Widmann, M., 2008. Mid- to late Holocene climate change: an overview. Quat. Sci. Rev. 27, 1791–1828. https://doi.org/10.1016/j.quascirev.2008.06.013.

Warken, S.F., Riechelmann, D.F.C., Fohlmeister, J., Schröder-Ritzrau, A., Frank, N., Scholz, D., Jochum, K.P., Mirea, I.-C., Constantin, S., Spötl, C., 2024. Dynamic processes determine precipitation variability in Eastern Central Europe since the last glacial maximum. Commun. Earth Environ. 5, 694. https://doi.org/10.1038/s43247-024-01876-9.

Weninger, B., Alram-Stern, E., Bauer, E., Clare, L., Danzeglocke, U., Jöris, O., Kubatzki, C., Rollefson, G., Todorova, H., Van Andel, T., 2006. Climate forcing due to the 8200 Cal yr BP event observed at early Neolithic sites in the Eastern mediterranean. Quat. res. 66, 401–420. https://doi.org/10.1016/j.yqres.2006.06.009.

Wickham, H., 2016. ggplot2: Elegant Graphics for Data Analysis. Springer, New York. https://ggplot2.tidyverse.org.

Wiegand, T., Moloney, A., 2004. Rings, circles, and null-models for point pattern analysis in ecology. Oikos 104, 209–229. https://doi.org/10.1111/j.0030-1299.2004.12497.x.

Xoplaki, E., Fleitmann, D., Luterbacher, J., Wagner, S., Haldon, J.F., Zorita, E., Telelis, I., Toreti, A., Izdebski, A., 2016. The Medieval climate anomaly and Byzantium: a review of the evidence on climatic fluctuations, economic performance and societal change. Quat. Sci. Rev. 136, 229–252. https://doi.org/10.1016/j.quascirev.2015.10.004.

Xoplaki, E., Luterbacher, J., Luther, N., Behr, L., Wagner, S., Jungclaus, J., Zorita, E., Toreti, A., Fleitmann, D., Izdebski, A., Bloomfield, K., 2021. Hydrological changes in late antiquity: Spatio-Temporal characteristics and socio-economic impacts in the Eastern mediterranean. In: Erdkamp, P., Manning, J.G., Verboven, K. (Eds.), Climate Change and Ancient Societies in Europe and the near East, Palgrave Studies in Ancient Economies. Springer International Publishing, Cham, pp. 533–560. https://doi.org/10.1007/978-3-030-81103-7_18.

Xoplaki, E., Luterbacher, J., Wagner, S., Zorita, E., Fleitmann, D., Preiser-Kapeller, J., Sargent, A.M., White, S., Toreti, A., Haldon, J.F., Mordechai, L., Bozkurt, D., Akçer-Ön, S., Izdebski, A., 2018. Modelling climate and societal resilience in the Eastern mediterranean in the last millennium. Hum. Ecol. 46, 363–379. https://doi.org/10.1007/s10745-018-9995-9.